Calculations of Xe line shapes in model nanochannels: Grand canonical Monte Carlo averaging of the ^{129}Xe nuclear magnetic resonance chemical shift tensor

Cynthia J. Jameson[a)]
Department of Chemistry M/C-111, University of Illinois at Chicago, Chicago, Illinois 60607-7061

(Received 26 November 2001; accepted 20 February 2002)

The nuclear shielding of the Xe atom is a tensor molecular electronic property that is a very sensitive indicator of the local environment. Xe atoms in nanochannels of a crystal exhibit anisotropic NMR line shapes that are characteristic of the average shielding tensor; the line shape is a manifestation of the systematic variation of the observed component of the tensor with the orientation of the nanochannel axis in the static uniform external magnetic field. In this paper, a method of calculating the Xe line shapes in nanochannels is presented. The averaging of the shielding tensor is carried out with a grand canonical ensemble at constant (μ, V, T). The line shapes are obtained by assuming a random distribution of orientations of the crystallites within a sample. The equivalent procedure is carried out by finding the component of the Xe shielding tensor along the magnetic field directions selected uniformly on the surface of a sphere. The approach developed here is used to predict the general behavior of Xe line shapes for Xe in elliptical channels of nanoscale dimensions. The channel architecture of crystalline aluminum phosphate ALPO-11 with dimensions 6.7×4.4 Å is used here as a model channel architecture. ALPO-11 is known to impose on Xe atoms an intermolecular NMR shielding response that is highly deshielded compared to a free Xe atom and with a line shape systematically changing with Xe occupancy [J. A. Ripmeester and C. I. Ratcliffe, J. Phys. Chem. **99**, 619 (1995)]. In the present work, model channels are constructed with Ne or Ar atoms in the ALPO-11 architecture, and grand canonical Monte Carlo simulations of Xe in these model channels are carried out. The difficulty lies in the construction of the Xe chemical shift tensor for each Xe in the channel at each configuration. We propose a new approach to calculations of the Xe chemical shift tensor in a nanochannel: the *additive dimer tensor model*. For a model nanochannel constituted entirely of rare gas atoms (Ne, for example) that are located at the crystallographic positions of the atoms constituting the channel walls, the Xe shielding tensor is determined as follows: For a given configuration of Xe atoms within the channel, the Xe shielding tensor of the Jth Xe atom at position (x_J, y_J, z_J) is calculated by a summation over all i of the contribution of $\mathrm{Xe}_J-\mathrm{Ne}_i$ dimer, the Ne atom located at the ith position, using the *ab initio* Xe–Ne rare gas dimer shielding tensor. To this is added the Xe–Xe contributions that are calculated by a summation over all L of the contribution of the $\mathrm{Xe}_J-\mathrm{Xe}_L$ dimer, using the *ab initio* Xe–Xe dimer shielding tensor. The systematic variations with Xe occupancy of the line shapes obtained from GCMC simulations using the additive dimer tensor model in the model Ne and Ar channels are used to provide general insight into the average Xe shielding tensor in nanochannels. The invariant qualitative aspects of the behavior of Xe line shapes in the model channels provide general predictions independent of the atoms constituting the channel. The chemical shift response of the Xe to the specific atoms constituting the channel walls provides the quantitative details. The specific application to Xe in ALPO-11 crystals compares favorably with experiment. © *2002 American Institute of Physics.* [DOI: 10.1063/1.1468884]

I. INTRODUCTION

The nuclear magnetic resonance (NMR) shielding σ is a molecular electronic property that is probed by a nuclear magnetic moment. The measurement of the property is straightforward: the probe nucleus reports back a frequency shift easily measured from a convenient reference signal from the same type of nucleus in a well-characterized environment (for example, the free atom) in the same external static magnetic field. The difference in frequency is a measure of the difference in the nuclear shielding between the system in question and the reference system, and this frequency difference is reported as a ratio to the reference frequency. Thus the ratio, the NMR chemical shift, is reported in ppm:

$$\delta = \text{chemical shift} = (\sigma_{\text{ref}} - \sigma_{\text{system}})/(1-\sigma_{\text{ref}}). \tag{1}$$

The nuclear shielding σ is a tensor property, with the indices referring to the components of the nuclear moment and magnetic field vectors. Thus, a nucleus in an oriented molecule (in a single crystal, for example) will provide different reso-

a)Electronic mail: cjj@sigma.chem.uic.edu

nance frequencies depending on the orientation of the molecular axes with respect to the external magnetic field that is static in the laboratory frame. As a molecular electronic property, the nuclear shielding has been studied by high resolution NMR spectroscopy as a function of density of molecules in the gas phase,[1] as a function of temperature in the limit of zero density;[2] its dependence on the masses of the atoms in the molecule[3,4] and on vibrational state or temperature[5] has provided a paradigm for other molecular electronic properties that are less well characterized experimentally and theoretically. The density dependence of the property in the gas phase introduced the concept of an intermolecular electronic property surface, a mathematical function of intermolecular distance and orientation. The mass dependence and temperature dependence in the limit of zero density of this property introduced the concept of an intramolecular shielding surface, a function of nuclear coordinates in the molecule (or a function of changes in bond lengths, bond angles, and torsion angles).[2] The molecular electronic property tensor is the nuclear shielding tensor; the measured tensor is the chemical shift tensor; they are uniquely related as written in Eq. (1), and we will be using both terms in this paper.

For the ^{129}Xe nucleus, the convenient reference system is the free Xe atom, which therefore has a chemical shift of zero ppm; any Xe resonance signal that is observed at a higher frequency than the free Xe atom has a positive chemical shift that arises from a more deshielded nucleus, i.e., $[\sigma(\text{free Xe atom}) - \sigma] > 0$.

Intermolecular interactions usually lead to deshielding of the Xe atom, an excellent model solute.[6–14] A few ^{129}Xe intermolecular shielding surfaces have been investigated, Xe–Xe,[15,16] Xe–Kr, Xe–Ar, Xe–Ne,[16] Xe–CH_4,[17] Xe–N_2, Xe–CO, Xe–CO_2,[18] and Xe–H_2O,[15] for example.

The components of the shielding tensor of each unique nuclear site can be measured from an oriented molecule such as in a single crystal mounted in a goniometer, by following the systematic change in the resonance frequency of the nuclear site as the crystal is rotated about a chosen axis. Alternately, the components of the shielding tensor can be measured using a polycrystalline powder where the random distribution of crystal axes orientations with respect to the external magnetic field provides a distribution of frequencies that are directly related to the components of the tensor along the magnetic field direction. The line shape that results from a polycrystalline sample is called a powder pattern. Information about the electronic environment of the nucleus is encoded in the shielding tensor, and can be the basis for unique assignments of molecular geometry. When the nuclear site is in a molecule that freely tumbles in solution or in the gas phase, only the trace of the shielding tensor determines the observed frequency. When the nuclear site is in a Xe atom that moves within confined spaces such as the nanochannels in a crystal, then some averaging of the tensor does occur, but the nanoscale dimensions of the confinement does not lead to isotropic averaging like that which occurs in a gas or liquid sample. Clearly, there is more information available in the full tensor associated with an anisotropic electronic environment than in the trace alone. In this paper we attempt to make a quantitative connection between the nature of the electronic environment in a nanochannel and the average Xe shielding tensor that is obtained from the NMR line shapes observed. We will be able to show which aspects of the observed Xe line shapes provide a signature of the channel architecture. We will answer the following question: What part of what is observed derives from the nature of the geometric confinement (i.e., the size and shape of the channel) and what part derives from the electronic structure of the atoms constituting the channel?

The NMR chemical shift of a Xe nucleus is a widely used probe of intermolecular interactions, structure of materials, distributions of sorbate molecules, and other phenomena.[12,13,19–23] In particular, the applications of Xe NMR to the characterization of nanocavities and nanochannels in crystalline materials[19,20] and nanostructures such as carbon nanotubes,[24] as well as the use of optically polarized ^{129}Xe nuclei to transfer its spin polarization to those particular protons in contact with Xe,[25–28] have exposed some fundamental problems relating to the distribution and dynamics of the Xe atoms within the nanopores. Only in rare instances does Xe remain highly localized at a minimum energy position in a pore. Examples are Xe in the small side pocket in mordenite[29] and in the cages of structure I clathrate hydrate,[30,31] where the Xe atom has a very sharp one-body distribution function. In this static picture, the Xe chemical shift tensor due to the interactions of the Xe atom with the atoms of the cage may be anisotropic; the observation of a line shape that is consistent with the distribution of orientations of a nonsymmetrical cage relative to the laboratory axis (the fixed external magnetic field direction) is easily understood.[32] Ripmeester and co-workers have discovered that experimental NMR line shapes of a single Xe atom guest in small cages in such clathrate hosts exhibit isotropic or axially symmetric characteristics.[30,33] The relatively temperature-independent Xe chemical shift is also an indication of the highly localized Xe position in the pore.[29] More usually, a single Xe atom in a nanopore of a crystalline material has a broad distribution function so that the observed NMR chemical shift of the Xe reflects an average over all interactions the Xe atom suffers within this distribution function. In the highly anisotropic environments of nanopores and nanochannels, where the confinement precludes isotropic averaging, one expects to observe a Xe NMR line shape that reflects the anisotropy of the environment. Anisotropic Xe line shapes for Xe in confined geometries have been reported since 1981, primarily by Ripmeester and co-workers.[30,33–41] A summary of some typical anisotropic tensor data is given in Table I.

The anisotropy of the Xe chemical shift that can be obtained experimentally for a single Xe atom in a nanopore (cavity or channel), sometimes with optically spin-polarized Xe at the limit of zero occupancy, should reflect the pore space geometry. Indeed, Ripmeester *et al.* have reported single scan experiments at extremely low occupancies for effectively a single Xe atom in ALPO-11 and in SSZ-24.[42,43] It has been suggested that NMR line shapes are capable of providing information about the geometry of a nanochannel, i.e., its dimensions and the symmetry of its cross section.[33]

TABLE I. Experimental values of average Xe shielding tensor components, ppm relative to σ(free Xe atom), at room temperature. $\Delta\sigma=(\sigma_{\parallel}-\sigma_{\perp})$ or $[\sigma_{\parallel}-\frac{1}{2}(\sigma_{\perp}+\sigma_{\perp'})]$.

System	σ_{iso}	$\Delta\sigma$	$\sigma_{\parallel}$	$\sigma_{\perp}$	$\sigma_{\perp'}$	Ref.
			Single Xe atom or zero loading			
Disk						
Xe in 5^{12} cage in clathrasil dodecasil-3C	−253	+45	−205	−250	···	33
Xe in 5^{12} cage-in clathrate hydrate II, 77 K	−225	+18	−213	−231	···	33
α-cyclodextrin fully hydrated	−192	+22.4	−177	−199.5	···	33
Xe in $5^{12}6^2$ cage in clathrate hydrate I, 265 K	−152	+32	−130.7	−162.7	···	34
						31
			Narrow-borrow pipe			
Zeolite SSZ-24	∼−62	∼−20	∼−75	∼−55	···	42, 43
TPP	−92.8	−33.1	−114.9	−80.2	−83.3	38
			Capped short pipe			
Xe in small cage β phenol clathrate	−229	−171	−343	−172.3	···	30
Xe in β quinol clathrate	−222	−160	−328.7	−168.7	···	30
			Medium-bore pipe			
ALPO-11	−114.4	−31	−135.1	−128.3	−79.8	35
ZSM-12	−76.7	−23.6	−92.4	−78.0	−59.7	41
			Medium loading			
			Narrow-bore pipe			
TPP	−109.2	∼0	−109.2	−109.2	−109.2	38
			Medium-bore pipe			
ALPO-11	−149	+20.9	−135.1	−177.3	−134.6	35
ZSM-12	−114.7	+16.3	−103.7	−127.0	−113.1	41
			Full loading			
			Narrow-bore pipe			
TPP	−119.0	+18.3	−106.8	−126.0	−124.3	38
			Medium-bore pipe			
ALPO-11	−183.2	+73.7	−134.1	−225	−190.5	35
			Capped short pipe			
DD3R		∼+70	∼−100	∼−170	···	36

Indeed, we have predicted for various channel types the qualitative nature of the Xe NMR line shapes by considering the relative magnitudes of the various components of the Xe shielding tensor and their magnitudes relative to the shielding of the free Xe atom.[32] Although the qualitative nature of the Xe NMR line shapes for these systems can be predicted by considering the static picture at the low-energy positions or adsorption sites, as have we have shown in an earlier paper,[32] only a grand canonical Monte Carlo (GCMC) or molecular dynamics (MD) simulation that appropriately includes the distributions of Xe positions within the nanochannel or cavity can provide the average chemical shifts as a function of orientation of the nanochannels with respect to the laboratory axis (or external magnetic field direction) for a single Xe atom in a nanochannel or in the limit of zero occupancy. This is what we propose to do here for the general case of Xe in a nanochannel and the specific case of Xe in ALPO-11. At the other extreme, in the limit of full occupancy, the anisotropy of the Xe chemical shift for the Xe atoms in a nanopore (cavity or channel), that can be observed even with thermally spin-polarized Xe, would, in addition, reflect the anisotropy of the Xe–Xe two-body distribution function within a nanochannel. The static picture of Xe atoms lined up in their respective minimum energy positions in the channel can be used to predict the qualitative nature of the line shapes that will be observed, as indeed we have demonstrated in Ref. 32. However, only a GCMC or MD simulation can provide a complete analysis of the observed Xe NMR line shapes and can reveal the separate Xe-channel and Xe–Xe contributions. This is what we intend to demonstrate in this paper, not just in these two limiting situations but for any general Xe occupancy of the channel.

II. METHODS

In an earlier paper,[32] we used *ab initio* Xe shielding calculations as the basis for predictions of average Xe chemical shift tensors in limiting situations such as Xe in a disk, or between flat parallel plates, or in circular pipes having a narrow or medium bore. We also predicted the Xe chemical shift tensor as a function of occupancy in elliptical pipes. All such predictions were based on *ab initio* shielding calculations in planar systems in static limiting situations such as Xe in the center of a ring of Ne atoms, or off center in the plane of a larger ring of Ne atoms, or alongside a linear molecule. Predictions of chemical shift tensors in fully occupied pipes were based on *ab initio* shielding calculations on three Xe atoms at various configurations with C_{2v} symmetry, varying angles all the way from 60° to 180°. Predictions for Xe chemical shift tensors in three-dimensional structures

were based on typical static arrangements of Xe within the channels, as dictated by symmetry and interaction energy considerations.[32] No calculations of Xe shielding tensor in three-dimensional channel structures have been carried out. The effect of dynamics or distributions within the three-dimensional channel structures to yield the observed average chemical shift tensor were not explicitly taken into account. In the present work, we explicitly include the averaging of the chemical shift tensor. Ideally one would do this by carrying out a molecular dynamics simulation over a long enough time that would span a large number of intrachannel diffusive steps of the Xe atoms such that the average obtained is relevant to the time scale of the MMR Experiment. This would be the appropriate procedure in cases where the diffusion is sufficiently slow that averaging throughout the entire channel could not be assumed, or else sufficiently fast that the Xe averaging between the gas phase outside and locations inside the channel can give rise to more complex ''exchange'' line shapes. In the situation that the diffusion within the channel is sufficiently fast and the channels are indefinitely long (so that no exchange with the gas phase is possible in the time scale of the NMR experiment), a Monte Carlo simulation would provide the same average as a very long MD simulation. Furthermore, a grand canonical Monte Carlo simulation can be carried out so that the average Xe occupancy would be generated by the simulation, rather than using an assumed occupancy number in a canonical MD simulation.

The use of grand canonical Monte Carlo simulations in calculations of average Xe isotropic chemical shifts were reported for the first time by us, using Xe in Na*A* zeolite as an example.[44] The isotropic chemical shifts are the values that would have been observed under spinning of the samples at the magic angle that effectively averages out all terms in the NMR Hamiltonian that have the $P_2(\cos\theta)$ dependence; these include the chemical shift tensor. For the present work, we have modified the simulations procedure so as to explicitly include the orientation of the external static magnetic field $\mathbf{B}_0$ relative to the static coordinates of the atoms constituting the crystal. Experimental samples are usually small crystallites rather than a single crystal. In a real experiment, the magnetic field of the NMR spectrometer is fixed in the laboratory and the crystalline axes of individual crystallites are randomly oriented at various directions. In our simulations, we use the equivalent approach, that is, we fix the crystal (simulation box) in the laboratory frame and place the $\mathbf{B}_0$ at various directions (θ, ϕ) in the Cartesian axis frame of the simulation box.

Let $\sigma^{B_0}(\theta,\phi)$ be the value, for a given Xe atom, of the Xe shielding tensor component along the direction of $\mathbf{B}_0$. The spectral intensity associated with an average nuclear shielding value $\langle\sigma^{B_0}(\theta,\phi)\rangle$, is proportional to the probability that the $\mathbf{B}_0$ vector lies in any infinitesimal solid angle $d\Omega$, that is, $d\Omega/4\pi=\sin\theta\, d\theta\, d\phi/4\pi$. At each configuration of some number of Xe atoms within the channel (the number of Xe atoms changes in a grand ensemble simulation), the calculation loops through the entire solid angle of 4π, taking steps of equal probability. Equal areas in the $\zeta\phi$ plane, taking $\zeta=-1$ to $+1$, $\phi=0$ to 2π, where $\zeta=-\cos\theta$, correspond to equal probabilities. For a given configuration we evaluate and accumulate all the values of $\sigma^{B_0}(\theta,\phi)$. The value of this component is given in terms of the Xe shielding tensor components $\sigma_{xx},\sigma_{xy},\ldots,\sigma_{zz}$, as follows:[45]

$$\begin{aligned}\sigma^{B_0}(\theta,\phi)=&\sigma_{xx}\sin^2\theta\cos^2\phi+\sigma_{yy}\sin^2\theta\sin^2\phi\\&+\sigma_{zz}\cos^2\theta+\tfrac{1}{2}(\sigma_{xy}+\sigma_{yx})\sin^2\theta\sin 2\phi\\&+\tfrac{1}{2}(\sigma_{xz}+\sigma_{zx})\sin 2\theta\cos\phi\\&+\tfrac{1}{2}(\sigma_{yz}+\sigma_{zy})\sin 2\theta\sin\phi.\end{aligned}\tag{2}$$

The first three terms in Eq. (2) are the same as found in standard texts (for example, Slichter's book[46]), corrected by the additional terms given by Hansen and Bouman.[45]

Averaging is obtained by Metropolis Monte Carlo generation of a large number of such configurations, constrained by a given temperature and Xe chemical potential equal to that in the bulk Xe gas phase in equilibrium with the adsorbed Xe in zeolite (or other crystalline material containing nanochannels or nanocavities), as described in Refs. 44 and 47. At high Xe occupancies, the acceptance ratio for random creation of a Xe atom becomes impractically small for the conventional Metropolis sampling using the standard Norman–Filinov generation of Markov steps. Thus, in this work, we use the more efficient sampling by the cavity-biased method of Mezei,[48] that we have used earlier for mixtures of Xe and Ar in zeolite Na*A*.[49]

To carry out the simulation, we need to specify the two functions: the tensor elements for a given Xe atom $\sigma_{xx},\sigma_{xy},\ldots,\sigma_{zz}$, as a function of configuration, and the potential energy of the system as a function of configuration. For the latter, the approach we use is a conventional one, i.e., we use pairwise additive potential energy functions, summing up over Xe–Xe pairs and Xe–O pairs. The V(Xe–Xe) function that we have used for Xe in zeolites is a fit to a Maitland–Smith form of the best empirical Xe–Xe pair potential by Aziz and Slaman.[44] For channels such as in the ALPO-11 crystal, in which only the oxygen atoms of the crystal framework are exposed to the Xe, the interactions of the Xe with the less accessible Al and P atoms of the ALPO-11 structure are ignored, and the entire interaction of each Xe with the nanochannel is described with a sum of V(Xe–O) cut-and-shifted pair functions.[50] For the model channels that we employ in this paper, we replace all the O atoms of the ALPO-11 structure with either Ne atoms or Ar atoms and we use the best available V(Xe–Ne) or V(Xe–Ar) pair potentials.[51,52]

The tensor elements $\sigma_{xx},\sigma_{xy},\ldots,\sigma_{zz}$, of a given Xe atom is difficult to characterize as a function of the configuration of all atoms in the simulation, even if we had the computational power to carry out very large *ab initio* calculations. Indeed, the symmetric part of the shielding tensor of one particular Xe atom, in general, would have six unique components and very general principal axes orientation since its environment has no symmetry. Here we propose a new approach to characterizing this Xe shielding tensor for an arbitrary configuration. We will call this approach the *additive dimer tensor model*.

For a model nanochannel constituted entirely of rare gas atoms (Ne, for example) that are located at the crystallographic positions of the atoms constituting the channel walls, for a given magnetic field $\mathbf{B}_0$ direction, for a given configuration of Xe atoms within the channel, we calculate the component along $\mathbf{B}_0$ of the Xe shielding tensor of the Jth Xe atom at position (x_J, y_J, z_J) as follows: First, the Xe-channel contribution is calculated by summing over all i the contribution of each $\mathrm{Xe}_J-\mathrm{Ne}_i$ dimer, for the Ne atom located at the ith position, using the component (along the $\mathbf{B}_0$ direction) of the *ab initio* Xe–Ne rare gas dimer shielding tensor. To this is added the Xe–Xe contribution, that is calculated as a sum over all L of the contribution of each $\mathrm{Xe}_J-\mathrm{Xe}_L$ dimer using the component (along the $\mathbf{B}_0$ direction) of the *ab initio* Xe–Xe rare gas dimer shielding tensor. Since the Xe shielding tensors have been calculated by us in the Xe–Rg (Rg = Xe, Kr, Ar, Ne) dimers as a function of the Xe–Rg distance over a wide range of separations,[16] this approach permits the calculation of the Xe shielding tensor component along a particular $\mathbf{B}_0$ direction for a particular Xe atom in any configuration of any number of Xe atoms within any nanochannel or nanocavity consisting of Rg atoms. Since the Xe shielding tensors and potential energy functions for the Xe–Rg dimers are known, we can therefore explore the Xe line shapes that may be expected as we change the cross-sectional area and the shape of the cross section of the nanochannel, as we tune the Xe shielding response to the channel wall atoms from the large deshielding response of the polarizable Ar atom (which is greater than that of the typical O atoms in nanochannel structures) to the smaller response of the ''harder'' Ne atom, and as we change the temperature. By using the Xe–Rg dimers, we also have the appropriate Xe–Rg potential functions that are *consistent* with the shielding functions, so that when used in generating the Metropolis-weighted configurations of Xe atoms, the simulations give rise to the grand canonical Monte Carlo averages over appropriate configurations for the types of channel atoms that give the Xe shielding response.

How good is the additivity of the dimer shielding tensor components along a $\mathbf{B}_0$ direction? We expect the results of this additive tensor model to be poor if the interactions that give rise to the shielding response are strong. For longer distances we have found reasonably good additivity. We found, for example, in examining the C_{2v} Xe_3 trimer,[32] that at angles 120° up to 180° the central Xe shielding component along the direction perpendicular to the plane of the three atoms, or along the C_2 axis of the Xe_3 trimer, calculated by assuming the additivity of dimer shielding tensors, deviate by only -2.3 to $+2.8$ ppm from the actual *ab initio* shielding value in the Xe_3 supermolecule, for the component that is around 5438 ppm at 4.0 Å, and only $+0.2$ to $+0.4$ ppm out of about 5560 ppm at 4.4 Å. The shielding component in the molecular plane and perpendicular to the C_2 axis deviates by only -0.1 to -0.5 ppm. All these deviations are down to 0.0 to 0.4 ppm at 4.4 Å. (These are the relevant distances since the $r_{\min}$ of the Xe–Xe dimer potential function is at 4.3627 Å.) Likewise, this additive dimer tensor model applied to Xe in the center of a circle of 8 Ne atoms at 4.0 Å deviates by only 0.16 ppm in one component, and 2.12 ppm in the other, compared to actual values obtained by *ab initio* calculations in the $\mathrm{Xe@Ne}_8$ supermolecule. (The $r_{\min}$ of the Xe–Ne dimer potential function is at 3.8661 Å.) When the Xe atom is placed 1.0 Å off center in the Ne_8 circle, such that the shortest Xe–Ne distance is 3.0 Å, the deviations of the model are 3.1, 0.32, and 0.14 ppm in the three components that are calculated *ab initio* to be changed by -40.0, -11.1, and -28.9 ppm from the shielding of the free Xe atom.[32] The magnitudes of these deviations are tolerable in comparison with typical Xe shifts of 50–300 ppm. The deviations come with either sign; therefore they do not necessarily accumulate when a large number of channel atoms and configurations are considered. The deviations from dimer tensor additivity are much more significant at much shorter distances,[32] however, these are distances that have smaller Metropolis probabilities since they involve Xe positions corresponding to repulsive regions of the potential.

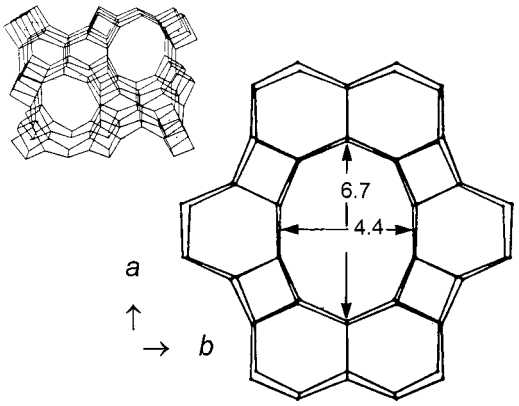

FIG. 1. The structure of a typical nanochannel: the ALPO-11 structure. These *a*, *b*, and *c* labels for the crystal axis directions are used in designating the tensor components in all the subsequent figures and the text of this paper. The effective cross section of the channel is based on assuming a diameter of 2.6 Å for an oxygen atom.

Our model nanochannel is constituted entirely of rare gas atoms (Ar or Ne) located at the crystallographic positions in ALPO-11, as an example of an elliptical pipe. The ALPO-11 structure is shown in Fig. 1. The simulation box consists of several unit cells that are static and fixed with respect to the laboratory axes, with the axis of the channel along the laboratory z axis. Periodic boundary conditions are used. At each generated configuration of Xe atoms within the channel, the calculations are done for magnetic field $\mathbf{B}_0$ fixed along 1140 unique (θ, ϕ) directions chosen equidistant in $\zeta\phi$ space. For the ith Ne atom of the channel the $\mathbf{r}_{\mathrm{XeNe}}$ vector is oriented at (θ_i, ϕ_i). Because dimers are used in this model, the contributions to the shielding tensors can be expressed entirely in terms of the two unique components $\sigma_\perp$ and $\sigma_\parallel$, for the dimer. For example, the contribution to the Xe shielding due to the ith Ne atom is given by the *ab initio* tensor component function evaluated at separation r_{XeNe}, $(\sigma_\perp, \sigma_\perp, \sigma_\parallel)_{\mathrm{XeNe}}$. The component along the $\mathbf{B}_0$ direction of this shielding at Xe_J, the Jth Xe atom located at position (x_J, y_J, z_J) due to the Ne_i atom is what we are looking for. That is,

$$\sigma^{B_0}(\text{due to } \mathrm{XeNe}_i) = (\sigma_\parallel)_{\mathrm{XeNe}} \cos^2\gamma + (\sigma_\perp)_{\mathrm{XeNe}} \sin^2\gamma, \tag{3}$$

where the $(\sigma_\parallel)_{\mathrm{XeNe}}$ is the dimer shielding tensor component parallel to the line of centers of the dimer at a separation $r_{iJ} = r(\mathrm{Xe}_J\mathrm{Ne}_i)$, and $(\sigma_\perp)_{\mathrm{XeNe}}$ is the component perpendicular to the line of centers. Here γ is the angle between the two vectors $\mathbf{r}_{\mathrm{XeNe}}$ oriented at (θ_i, ϕ_i) relative to the laboratory z axis and $\mathbf{B}_0$ oriented at (θ, ϕ) with respect to the laboratory z axis. Thus,

$$\cos\gamma = \sin\theta\cos\phi\cdot[(x_i - x_J)/r_{iJ}] + \sin\theta\sin\phi \cdot[(y_i - y_J)/r_{iJ}] + \cos\theta\cdot[(z_i - z_J)/r_{iJ}]. \tag{4}$$

In this additive dimer tensor model, we assume that we can calculate the Xe–Xe contributions to the shielding of the Jth Xe atom by using a summation over the contributions of Xe–Xe dimers, using the *ab initio* XeXe dimer shielding function in each case. For example, for the Lth Xe atom located at (x_L, y_L, z_L) the $\mathbf{r}_{\mathrm{XeXe}}$ vector is oriented at (θ_L, ϕ_L) relative to the laboratory z axis. The contribution to the Xe shielding due to this Xe atom is given by the *ab initio* tensor component function $(\sigma_\perp, \sigma_\perp, \sigma_\parallel)_{\mathrm{XeXe}}$ evaluated at a separation $r_{LJ} = r(\mathrm{Xe}_J\mathrm{Xe}_L)$. The component of this shielding at Xe_J due to Xe_L along the $\mathbf{B}_0$ direction is what we are looking for. That is,

$$\sigma^{B_0} = (\text{due to } \mathrm{XeXe}_L) = (\sigma_\parallel)_{\mathrm{XeXe}} \cos^2\gamma + (\sigma_\perp)_{\mathrm{XeXe}} \sin^2\gamma, \tag{5}$$

where γ is the angle between the two vectors $\mathbf{r}_{\mathrm{XeXe}}$ oriented at (θ_L, ϕ_L) relative to the laboratory z axis and $\mathbf{B}_0$ oriented at (θ, ϕ) with respect to the laboratory z axis.
The $\cos\gamma$ for $\mathrm{Xe}_L - \mathrm{Xe}_J$ contributions to the Xe shielding of the Jth Xe nucleus is obtained by

$$\cos\gamma = \sin\theta\cos\phi\cdot[(x_L - x_J)/r_{LJ}] + \sin\theta\sin\phi \cdot[(y_L - y_J)] + \cos\theta\cdot[(z_L - z_J)/r_{LJ}]. \tag{6}$$

The polycrystalline powder line shape results when the ensemble averages $\langle\sigma^{B_0}(\theta,\phi)\rangle$ are binned into a histogram. At the same time the GCMC simulations provide the Xe chemical shifts that would be observed in a single crystal experiment. Upon rotation of a single crystal containing Xe about the various axes of the crystal, the observed single peak will have a frequency corresponding to $\langle\sigma^{B_0}(\theta,\phi)\rangle$. Thus, to find the chemical shifts that would be observed in a single crystal experiment, we can use the same GCMC results as those used to display the polycrystalline powder line shape. For example, upon rotation about the x axis of the crystal (the long axis of the ellipse in the case of ALPO-11), we should observe $\langle\sigma^{B_0}(\theta, \phi = \pi/2)\rangle$. Upon rotation about the y axis of the crystal (the short axis of the ellipse in the case of ALPO-11), we should observe $\langle\sigma^{B_0}(\theta, \phi = 0)\rangle$. Upon rotation about the z axis of the crystal (the channel axis in the case of ALPO-11), we should observe $\langle\sigma^{B_0}(\theta = \pi/2, \phi)\rangle$.

In all the work reported here, the assumption is that the system is a sealed sample in which the adsorbed Xe is in equilibrium with the overhead Xe gas, the occupancy being determined by the Xe chemical potential being the same in both phases. The channels are assumed to be indefinitely long so that in the time scale of the NMR experiment there is no exchange between the Xe in the bulk gas and the Xe within the nanochannels or between Xe atoms in different nanochannels. In the GCMC procedure, the ensemble averages $\langle\sigma^{B_0}(\theta,\phi)\rangle$ can be obtained in several ways, according to the assumed Xe dynamics. If Xe diffusion is assumed to be sufficiently fast, then each Xe atom has a chance to experience all the Xe environments within one nanochannel. This would result in a complete averaging throughout the channel, which is simulated by accumulating all the $\sigma^{B_0}(\theta,\phi)$ contributions for a given (θ, ϕ) from all the Xe atoms throughout the simulation; only at the end of the simulation are these values of shielding binned into the spectral display. In the simulation, the separate contributions can be accumulated separately: the Xe–channel interactions to the average Xe shielding tensor, the Xe–Xe contributions, and the total shielding tensor. A consequence of binning into the spectral display only at the end of the simulation is that the coarseness of the histogram is determined by the number of (θ, ϕ) values used. The finite number of (θ, ϕ) values used may not be large enough, resulting in a coarse spectral histogram, as shown in Fig. 2(a). Assigning a Lorentzian shape to the spectral peak at each bin leads to a more realistic spectral shape, as shown in Fig. 2(b). Some ripples may remain, nevertheless, which could be smoothed over by using somewhat larger Lorentzian linewidths, if desired. In Fig. 2 both the

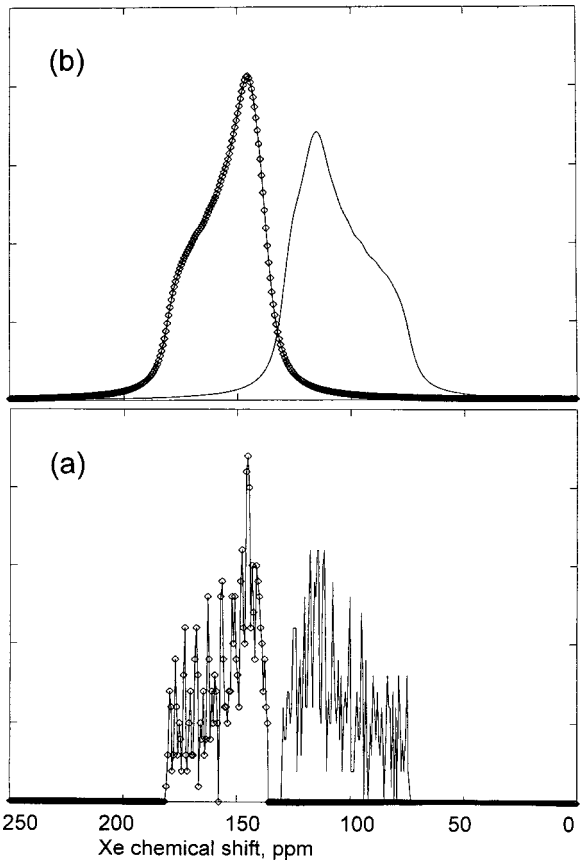

FIG. 2. (a) The spectral histogram resulting from a GCMC simulation, and (b) the broadened line shape obtained by using Lorentzian functions of uniform width to represent each bar of the histogram. The Xe–channel contribution (shown without points) is displayed together with the total spectrum (shown with points).

total spectrum and the spectrum resulting from only the Xe–channel interactions are shown. Experimental results obtained at room temperature in an ALPO-11-type structure should be compared with the spectra simulated from the complete averaging throughout the channel.

If, on the other hand, the diffusion is assumed to be limited to a small number of Markov steps n_M, then, after every n_M step the $\sigma^{B_0}(\theta,\phi)$ contributions for all the Xe atoms that are within a specified distance parameter (diffusion length) of one another are averaged together and binned into the spectral display for a given (θ, ϕ). Throughout the simulation the diffusion averaged spectral display accumulates intensity. This results in a ''diffusion-averaged'' spectrum. The spectra resulting from the complete averaging throughout the channel and the diffusion averaged spectra can be different. Obviously, when the number of Markov steps n_M are few enough, the resulting spectrum would be the same as for a quenched sample of Xe in a zeolite, that is, one instantaneously taken down to a very low temperature, where each Xe is effectively immobilized, an artifactual metastable state leading to an exceedingly broad spectrum, since every single Xe atom reports the unique shielding at the environment it finds itself. Diffusion-averaged spectra from the GCMC simulations are less coarse than those resulting from the complete averaging throughout the channel, since the values $\sigma^{B_0}(\theta,\phi)$ are binned more frequently into the spectral display. In Monte Carlo simulations the diffusion length is merely a parameter that is difficult to associate with temperature and Xe occupancy without additional experimental information. Molecular dynamics simulations would provide a more appropriate average when the sample morphology or the NMR experiment is diffusion limited.

III. RESULTS FOR MODEL SYSTEMS: Ne AND Ar CHANNELS

We can use our model systems to generate quantitative results for the general behavior of the anisotropic Xe NMR line shape under various conditions. Since the additivity of intermolecular shielding is assumed in our approach, the simulation permits the separate binning of spectral display for the Xe–channel contributions only, the Xe–Xe contributions only, as well as the total Xe shielding tensor. We can explore how the changes in the line shape (i.e., the average shielding tensor components) of Xe–channel intermolecular shielding and Xe–Xe intermolecular shielding can result from variation of the size and polarizability of the atoms of the channel from Ne to Ar. Ne and Ar channels give different Xe shielding responses and also different potential energy surfaces for a single Xe interacting with the channel walls. Indirectly, the Xe–channel interactions also affect the two-body Xe–Xe distribution function that determines the Xe–Xe contributions to the shielding tensor. We can explore how large this effect can be by changing the channel atoms from Ne to Ar. We can also explore how the changes in the line shape can result from changing Xe occupancies (i.e., filling up the channel), and whether the changes in the line shape with occupancy can be used as an indicator of the structure of the channel. Many crystalline materials with nanochannels and nanocavities have isomorphic structures; for example, the aluminum phosphate ALPO-5 and the silicate SSZ-24 are isomorphic structures, with Si replacing both Al and P atoms in the highly siliceous version of SSZ-24. What features of the Xe line shape are due to the structure of the channel, and how much does the line shape change when the electronic structure of the oxygens that constitute the channel walls are changed, without changing the architecture of the channel? By tuning the Xe-channel interaction between the two extremes of Ne channels and Ar channels, for the identical channel geometry (same atomic positions), we can explore the influence of the electronic structure of the channel atoms on the Xe NMR line shape. We describe these model studies below. In future work we can also explore the effect of changing temperature while comparing results at the same occupancy, the effect of changing the geometric constraints, i.e., the channel architecture, without changing the electronic structure of the constituent atoms. We can do this by comparing the ALPO-5 structure, the ALPO-11 structure, the carbon nanotube structure, etc., where the channel cross section changes and the channel wall pattern changes, but the electronic structure of the constituent atoms can be kept fixed at either Ne or Ar or something in between.

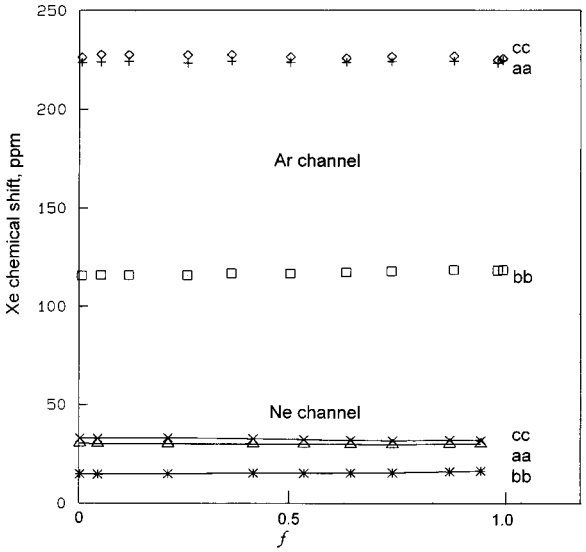

FIG. 3. GCMC simulations provide the contributions of Xe–channel interactions to the Xe NMR chemical shift tensor for Xe in the model Ne channel and in the model Ar channel at various fractional occupancy. The value of f is the average number of Xe atoms per unit cell divided by the maximum occupancy, which is four per unit cell.

In this paper we consider a fixed channel architecture, that of ALPO-11. It is consistent with the assumed additivity of intermolecular Xe shielding contributions to the shielding tensor, and it serves our purpose to examine the Xe–Xe intermolecular shielding contributions separately from the Xe–channel contributions. First, let us observe the effect of the electronic structure of the channel wall atoms on the spectral line shape coming from the Xe–channel interactions alone. We consider the Xe shielding response to model channels constituted of relatively small, less polarizable Ne atoms or relatively larger, more polarizable Ar atoms arranged in an ALPO-11 channel structure. We display in Fig. 3 only the

Xe–channel contributions to the NMR line shape. As defined in Eq. (1), the shielding (the molecular electronic property) and the chemical shift (the observed frequency shift from the reference substance, the free Xe atom) are related. Thus, in the figures in this paper we display the chemical shifts. For example, in Fig. 3 the average chemical shifts tensor components are

$$\sigma(\text{free Xe atom}) - \langle \sigma^{B_0}(\text{Xe channel}) \rangle_{\alpha\alpha},$$

$\alpha\alpha = cc$, *aa*, *bb*, respectively, for components along the channel axis, along the long and the short axis of the elliptical cross section.

The results shown in Fig. 3 provide the following insights: First, the anisotropy of the Xe shielding tensor coming from the Xe-channel interactions alone clearly indicates three unique components of the tensor. The nonaxial nature of the Xe tensor (three nonequivalent components) is consistent with the fact that the channel is approximately an elliptical cylinder, as seen in Fig. 1. The two average tensor components perpendicular to the channel axis are nonequivalent. Second, the component along the channel axis is the most deshielded component (the largest positive chemical shift with respect to the isolated Xe atom reference system), for the model Ne channel as well as the Ar channel. Third, where the indices *a*, *b*, *c* correspond to the crystalline directions in the ALPO-11 structure, *c* being the direction of the channel axis, and *a* is perpendicular to this axis and along the long axis of the ellipse, we find that the relative order of the three components of the Xe-channel tensor is preserved in both the Ne channel and the Ar channel,

$$\begin{aligned} \langle \sigma^{B_0}(\text{Xe channel}) \rangle_{cc} &< \langle \sigma^{B_0}(\text{Xe channel}) \rangle_{aa} \\ &< \langle \sigma^{B_0}(\text{Xe channel}) \rangle_{bb} \\ &< \sigma(\text{free Xe atom}), \end{aligned}$$

where the values are all deshielded (negative) relative to the free Xe atom. In other words, the chemical shift tensor components increase in the order

$$\begin{aligned} \langle \delta_{bb}(\text{Xe channel}) \rangle &< \langle \delta_{aa}(\text{Xe channel}) \rangle \\ &< \langle \delta_{cc}(\text{Xe channel}) \rangle, \end{aligned}$$

whether the channel is constituted of Ne atoms or Ar atoms. We previously predicted this relative order using only static configurations.[32] In this work we present, for the first time, a proper averaging of the tensor over Xe configurations in the channel. The results indicate, as already foreseen in our earlier work,[32] that the relative order of Xe shielding tensor components, measured experimentally from the line shape at nearly zero Xe occupancy, is a signature of the channel architecture. We also note that the span of the NMR line shape (the shielding difference between the least shielded component and the most shielded component) is a very sharp indicator of the differences in shielding response between a Xe in a Ne channel and a Xe in an Ar channel. The Xe shielding response is to greater deshielding in an Ar channel,

$$\begin{aligned} \langle \sigma^{B_0}(\text{Xe–Ar channel}) \rangle_{cc} &< \langle \sigma^{B_0}(\text{Xe–Ne channel}) \rangle_{cc} \\ &< \sigma(\text{free Xe atom}), \end{aligned}$$

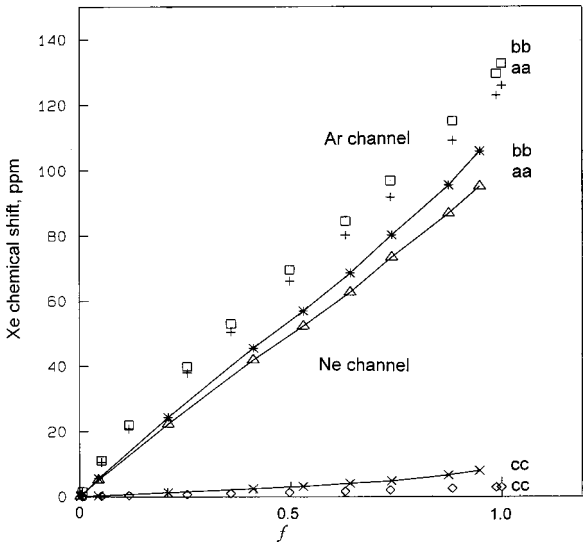

FIG. 4. The anisotropy of the average chemical shift tensor resulting from the contributions from the Xe–Xe interactions alone, as the Xe occupancy is increased from effectively zero to full occupancy in the model Ne channel, and in the model Ar channel.

for the *cc* component, and the same goes for the *aa* and *bb* components. The Xe–channel contributions to the chemical shift tensors with a free Xe atom as a reference,

$$\langle \delta_{cc}(\text{Xe–Ne channel}) \rangle < \langle \delta_{cc}(\text{Xe–Ar channel}) \rangle;$$

they differ by a factor of about 3. While the relative order of the three components is only a function of the ALPO-11 architecture, the isotropic chemical shift and the magnitudes of the three components, and therefore the Xe lineshape in the limit of zero occupancy, are sensitive measures of the electronic structure of the constituent atoms of the channel.

The average fractional occupancy of the channel is here written in terms of *f*, the average number of Xe atoms per unit cell divided by the maximum occupancy number, which is four Xe atoms per unit cell. We find in Fig. 3 that there is very little change in the Xe–channel interactions with increasing occupancy of the channel, whether the channel is constituted of Ne atoms or Ar atoms. This was not the case for Xe atoms inside a nanocavity of zeolite Na*A*, where we had found that the Xe chemical shift contributions coming from the Xe–wall interactions increased with Xe occupancy.[53] The presence of a higher number of Xe atoms in an open-ended channel does not preclude any one Xe from experiencing the entire intrachannel volume in the same way as does a single Xe alone in the channel. The small change with occupancy is more obvious at 150 K than at 300 K.

Now let us consider the average Xe–Xe intermolecular shielding tensor. Is information about the architecture and constitution of the channel encoded into it and how? Figure 4 shows the shielding tensor arising from the Xe–Xe intermolecular shielding alone, as the Xe occupancy is increased from effectively zero to full occupancy. The changes in the average shielding tensor (coming from the Xe–Xe part alone) with increasing Xe occupancy are very similar for the Ne channel and the Ar channel. We find that the anisotropy of the Xe–Xe intermolecular chemical shift tensor is consis-

tent with the geometry of the channel. In other words, for the given channel architecture, the anisotropy due to the Xe–Xe interactions and its dependence on Xe occupancy is qualitatively the same for the same channel architecture, irrespective of the stronger or weaker Xe interactions with the constituent atoms of the channel. For the Xe–Xe intermolecular shielding tensor, the order of the components is the reverse of the Xe–channel tensor, and is the same for the Ne and Ar channels,

$$\langle \delta_{cc}(\mathrm{Xe\text{–}Xe})\rangle \ll \langle \delta_{aa}(\mathrm{Xe\text{–}Xe})\rangle < \langle \delta_{bb}(\mathrm{Xe\text{–}Xe})\rangle,$$

that is, the most deshielded component is $\langle \sigma^{B_0}\rangle_{bb}$, along the short axis of the channel cross section. The Xe–Xe intermolecular shielding tensor component parallel to the channel axis itself is hardly different from the free Xe atom: $\{\sigma(\text{free atom})\text{-}\langle \sigma^{B_0}\rangle_{cc}\}$ is zero to 8 ppm in the Ne channel and zero to 3 ppm in the Ar channel. That is, for any Xe occupancy number,

$$\{\langle \delta_{cc}(\mathrm{Xe\text{–}Xe})\rangle\}_{\mathrm{Ar\ channel}} < \{\langle \delta_{cc}(\mathrm{Xe\text{–}Xe})\rangle\}_{\mathrm{Ne\ channel}}.$$

This is the expected case for channels that have cross sections small enough that Xe atoms cannot pass each other in the channel. The somewhat larger $\langle \delta_{cc}(\mathrm{Xe\text{–}Xe})\rangle$ in the Ne channel than in the Ar channel arises from the Ne channel cross section being effectively larger than when the channel is constituted by Ar atoms. The other two components in the plane perpendicular to the channel axis are comparable to each other, markedly deshielded compared to the component along the channel axis, and in the same relative order, i.e., $\langle \sigma^{B_0}\rangle_{bb}$ more deshielded than $\langle \sigma^{B_0}\rangle_{aa}$, irrespective of the atoms constituting the channel wall. The same changes with the average occupancy occur in both the neon and argon channels. There is a systematic significant difference between having a channel of Ne atoms compared to a channel of Ar atoms, however. For any given Xe occupancy number,

$$\{\langle \delta_{aa}(\mathrm{Xe\text{–}Xe})\rangle\}_{\mathrm{Ne\ channel}} < \{\langle \delta_{aa}(\mathrm{Xe\text{–}Xe})\rangle\}_{\mathrm{Ar\ channel}};$$

the same holds for the *bb* component, and both are in the opposite direction from the *cc* component. The Xe atoms can get closer to the walls of a Ne channel than to the walls of an Ar channel, effectively allowing the Xe–Xe interactions a larger volume; longer average Xe–Xe distances for intermolecular shielding lead to smaller magnitudes of deshielding relative to the free Xe atom. This is the reason for the systematic differences (seen in Fig. 4) in the Xe–Xe contribution as a function of occupancy in the two model channels. With increasing occupancy, pronounced deshielding occurs along the two axes lying in the cross-sectional plane in a predictable way. The change is not linear with fractional occupancy, and if one looks closely, there is a slight sigmoid trend with increasing occupancy. The sigmoid trend is more pronounced in the neon channel and is more pronounced at 150 K compared to 300 K. (We will not consider temperature effects in this paper.) The choice of the V(Xe channel) potential energy function affects the Xe–Xe part of the shielding tensor indirectly, in that the pair distribution function $g(r_{\mathrm{Xe\text{–}Xe}})$ is affected by the choice of V(Xe channel). Therefore, in order to calculate the Xe–Xe part of the shielding tensor, we must have a reasonable representation of the fluid–wall interaction energies. Note that the change in electronic structure in going from Ne to Ar in these model channels is more pronounced than the small changes in the electronic structure of oxygen atoms in going from ALPO-11 to the silicate version SAPO, or in going from the aluminum phosphate ALPO-5 to the silicate SSZ24 with the same architecture.

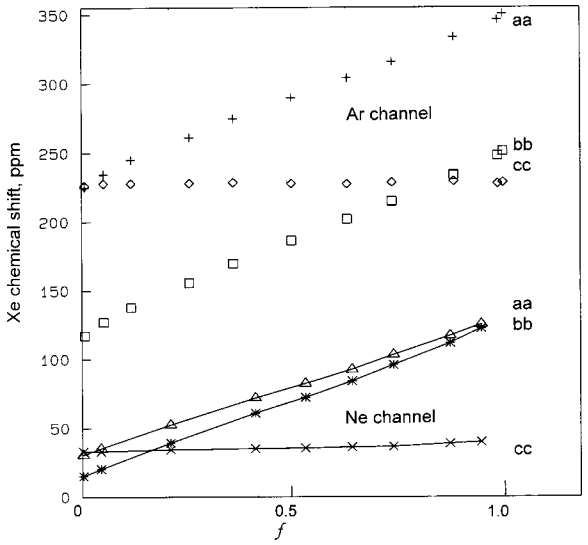

FIG. 5. Average chemical shift tensor components of the total spectrum, as a function of Xe occupancy in the model Ne and Ar channels.

By analyzing the separate contributions from the Xe channel and Xe–Xe to the line shape, we provide a better understanding of how the nature of the channel influences the two separate parts. In summary, the qualitative anisotropy of the Xe tensor (the number of unique components, and their relative order) at zero occupancy is a measure of the shape of the channel cross section; the quantitative anisotropy is a measure of the polarizability of the atoms constituting the channel, or more precisely, their ability to elicit a Xe shielding response. On the other hand, the Xe–Xe contribution to the tensor has a qualitative anisotropy (the number of unique components and their relative order) that is also determined by the architecture of the channel, and the dependence on Xe occupancy of its tensor components are affected indirectly by the constitution of the channel due to the different $g(r_{\mathrm{Xe\text{–}Xe'}})$ pair distribution that is imposed by the Xe–channel interactions. Thus, both the fluid–fluid and the fluid–wall parts of the Xe shielding tensor have predictable qualitative behavior from the channel architecture alone.

Figure 5 shows the average shielding tensors of the total spectrum that results from the two contributions, as a function of occupancy. The Xe NMR spectra in the Ne channel and in the Ar channel appear superficially very different, for the reasons already noted in the separate contributions. Nevertheless, the general qualitative behavior is the same whether the channel is constituted of Ne atoms or Ar atoms: (1) one component remains essentially constant, (2) the other two components are distinct from each other and both increase with Xe occupancy, (3) one of the latter two components increases somewhat faster, and (4) all the tensor components are easily unequivocally assignable with respect to

the crystal axis directions. These general trends of the tensor components are the consequences of having a channel structure with an elliptical cross section, and a cross section small enough that Xe atoms cannot pass each other. Qualitatively, with increasing Xe occupancy, the $\langle\delta\rangle_{cc}$ changes very little in both model channels, whereas the $\langle\delta\rangle_{aa}$ and the $\langle\delta\rangle_{bb}$ change greatly in the same direction as the isotropic chemical shifts. However, because of the starting tensor components at near-zero Xe occupancy being very close to each other in the Ne channel, the changes due to increasing anisotropy of the Xe–Xe part results in the $\langle\sigma\rangle_{aa}$ and $\langle\sigma\rangle_{bb}$ components being on the same side of the nearly constant component $\langle\sigma\rangle_{cc}$, thus resulting in quite a different total line shape at full occupancy in the Ne channel than is found for the Ar channel. Also, the span of the Xe spectrum in the Ne channel starts out small at zero occupancy and increases dramatically toward full occupancy. On the other hand, the very large anisotropy at near-zero occupancy of Xe in an Ar channel ($\langle\sigma\rangle_{cc}$ being very deshielded compared to $\langle\sigma\rangle_{bb}$ when nearly empty) leads to a large span at very low occupancy and a comparable, even a slightly smaller overall span at full occupancy. The tensor appears pseudoaxially symmetric at two occupancies in the Ar as well as the Ne channel. Unless experiments are conducted over a range of occupancy numbers in a nanochannel, a false conclusion about the symmetry of the channel may result.

One could examine the changes in the isotropic chemical shifts, as well. These are the values of $(\frac{1}{3})$ of the sum of the three individual components. Although there is much change in the isotropic chemical shifts that provides some indications about the nature of the channel, it is clear that the individual tensor components provide more complete information and understanding.

In summary, the simulations in these model channels provide the following insight that we will express uniformly in terms of the chemical shift δ (rather than the shielding σ).

(1) The average Xe chemical shift tensor under conditions of nearly zero occupancy is a signature of the channel architecture. The number of distinct components and the relative order of the principal tensor components (i.e., the assignments of the components to the crystal axes) for any elliptical nanochannel at near-zero occupancy is
$\langle\delta\rangle_{bb}<\langle\delta\rangle_{aa}<\langle\delta\rangle_{cc}$,
where c is the channel axis direction, and a is the longer axis of the elliptical cross section. In other words, the tensor components from the spectrum are easily unequivocally assignable with respect to the crystal axis directions.

(2) The Xe–channel contributions to the average chemical shift tensor are nearly independent of the Xe occupancy.

(3) The Xe–Xe contributions to the average chemical shift tensor has a relative order of components that are exactly opposite to that of the Xe–channel contribution, i.e.,
$\langle\delta\rangle_{cc}<\langle\delta\rangle_{aa}<\langle\delta\rangle_{bb}$.

(4) This relative order of the Xe–Xe contributions to the tensor is maintained for any Xe occupancy from nearly zero up to full, *provided the channel cross section is small enough that Xe atoms cannot pass each other in the channel*, in which case the component along the channel axis $\langle\delta\rangle_{cc}$ is also very different from the other two components, in that it is small (shielding is nearly unchanged from the free Xe atom), and changes very little and in the same direction as the other two components.

(5) The effective size of the atoms constituting the nanochannel influences the Xe–Xe contribution to the tensor. Larger atoms lead to larger magnitudes of the Xe–Xe chemical shift tensor components.

(6) The effective polarizability of the constituent atoms determine the magnitude of the Xe shielding response and therefore determine the magnitudes of the individual tensor components that will be observed at nearly zero occupancy.

(7) The total average chemical shift tensor that is observed, being a sum of Xe–channel and Xe–Xe contributions, reflects the channel architecture in the number of unique components, and the number is unaffected by the atomic constitution of the channel.

(8) That component of the average chemical shift tensor parallel to the channel axis remains nearly invariant with occupancy number (*provided the channel cross section is small enough that Xe atoms cannot pass each other in the channel*).

(9) The relative order of the tensor components (i.e., the assignments of the components to the crystalline axes) do change with occupancy, a consequence of the fact that the magnitudes of the individual tensor components change with occupancy in a systematic way that is nearly independent of the nature of the atoms constituting the channel.

(10) The two components of the total chemical shift tensor perpendicular to the channel axis remain in the same relative order with each other, both increasing with increasing Xe occupancy in the channel, one component (that one along the short axis of the elliptical cross section, $\langle\delta_{bb}\rangle$) increasing at a slightly faster rate than the other, so that the two components, changing with occupancy in a nearly parallel fashion, nevertheless tend slightly toward each other with increasing occupancy.

IV. A MODEL FOR THE σ(Xe–O_{zeol}) DIMER SHIELDING TENSOR FUNCTION

As atomic models for the bridging oxygen atoms of the ALPO-11 channel, Ne and Ar are at extremes. Ne provides too small a shielding response and gives a potential minimum for the Xe that is too close to the walls. On the other hand Ar provides somewhat too large a Xe shielding response and gives a potential minimum that is a bit too far away from the walls and may be too deep. The distance dependence of the Xe–O shielding tensor functions and the Xe–O potential functions are intimately connected. In order to describe the Xe–O_{zeol} shielding contributions with an appropriate dimer model, we have to scale the distance depen-

dence of both functions in the same way, so as to have an internally consistent description of the average Xe shielding response from the channel. One way in which we can systematically tune the Xe shielding tensor from the Ne channel to the Ar channel to find the suitable one for an O_{zeol} channel is to take the Xe–Ar shielding tensor and scale it to the appropriate distance r_0 for the zeolite in question. This idea is based on the finding that the shielding functions for the rare gas pairs do scale in their distance dependence according to r_0 of the potential functions. For example, we have found that the Xe–Xe, Xe–Kr, Xe–Ar, and Xe–Ne shielding functions have a nearly universal form in those parts of the range of r that are accessible at ordinary temperatures, say from $r=0.85r_0$ to very large distances, and a response scaling factor that is approximately given by a product of constants.[16] Thus, we can consider developing a dimer shielding tensor function for $Xe–O_{zeol}$ by applying this type of scaling to the *ab initio* shielding tensor for the Xe–Ar dimer. In Fig. 6 we show the NMR line shapes arising from Xe–channel intermolecular shielding for Xe in several model channels having the ALPO-11 structure. Xe in channels that are constituted of Ar-like atoms scaled down to $r_0=3.5$ Å in Fig. 6(d) and $r_0=3.4$ Å in Fig. 6(c), are compared to Xe in a channel constituted of Ne atoms in Fig. 6(a), and of Ar atoms in Fig. 6(e). We see that tuning the Xe-shielding tensor function down to $r_0=3.4$ Å from the $r_0=3.6454$ Å of the best available Xe–Ar potential function[52] leads to a line shape that is already quite similar to the experimental spectrum of Xe in ALPO-11 reported by Ripmeester and Ratcliffe at the very low (9.6%) occupancy.[35,42]

Another approach to the $Xe–O_{zeol}$ dimer shielding tensor function is to start from the isotropic shielding function $\sigma_{iso}(Xe–O_{zeol})$, if we had such a function. Consistent with our general approach based on dimer shielding tensors, we consider such an isotropic shielding function that is characteristic of all the O atom types in a zeolite taken together, as if it were the isotropic shielding function of some Xe–O dimer. The parallel and perpendicular components of the Xe–Rg (Rg=Ne,Ar,Kr,Xe) dimer shielding tensors are related to the isotropic Xe–Rg shielding in a simple way. This relation is made obvious by considering the Ramsey partitioning of the shielding tensor into paramagnetic and diamagnetic parts.[54] The first is written in terms of the angular momentum operators that mix excited electronic states with the ground electronic state due to the presence of either the perturbation of the external magnetic field or the nuclear magnetic moment. The second can be written simply in terms of matrix elements involving only the electronic ground state. For a *linear* diamagnetic molecule or supermolecule, the paramagnetic part of the shielding tensor is identically zero along the direction parallel to the line of centers. Thus,

$$\sigma_{\parallel}=\sigma_{\parallel}^{\mathrm{diam}}, \tag{7}$$

$$\sigma_{\perp}=\sigma_{\perp}^{\mathrm{diam}}+\sigma_{\perp}^{\mathrm{param}}, \tag{8}$$

$$\sigma_{\mathrm{iso}}=(\tfrac{1}{3})\{2\sigma_{\perp}+\sigma_{\parallel}\}$$
$$=(\tfrac{1}{3})\{2\sigma_{\perp}^{\mathrm{diam}}+2\sigma_{\perp}^{\mathrm{param}}+\sigma_{\parallel}^{\mathrm{diam}}\}. \tag{9}$$

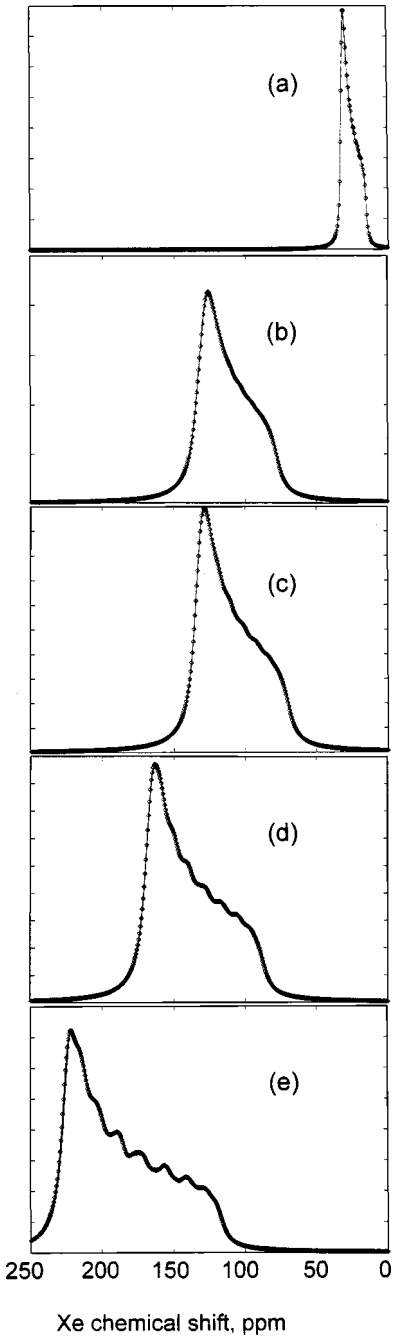

FIG. 6. The Xe NMR spectrum at nearly zero occupancy for Xe in model channels of ALPO-11 structure (a) consisting of Ne atoms, (b) consisting of O atoms characteristic of aluminosilicates with a 1:1 Si/Al ratio, (c) consisting of Ar-like atoms scaled down to $r_0=3.4$ Å, (d) scaled down to $r_0=3.5$ Å, and (e) consisting of Ar atoms.

Thus, the two unique components of the shielding tensor of a linear molecule can be written as

$$\sigma_{\perp}=(\tfrac{3}{2})\sigma_{\mathrm{iso}}-(1/2)\sigma_{\parallel}^{\mathrm{diam}}, \tag{10}$$

$$\sigma_{\parallel}=\sigma_{\parallel}^{\mathrm{diam}}. \tag{7}$$

We know from our *ab initio* shielding tensor calculations of Xe in rare gas dimers that the parallel component of the tensor $\sigma_{\parallel}$ differs from σ (a free Xe atom) by a positive, small amount that varies with distance in a simple way. Thus, if we know the isotropic shielding $\sigma_{iso}(Xe–O_{zeol})$, or the differ-

ence $[\sigma_{\rm iso}(\mathrm{Xe–O_{zeol}})-\sigma(\text{free Xe atom})]$, as a function of distance, we can obtain the individual tensor components as a function of distance provided that we have a good, even if approximate, method of finding $\sigma_{\parallel}^{\rm diam}$. Flygare and Goodisman have actually provided such a method:[55]

$$\sigma_{\parallel}^{\rm diam}(\mathrm{Xe–O})\approx\sigma_{\parallel}^{\rm diam}(\text{free Xe atom}) + (\tfrac{2}{3})\langle\rho^2\rangle_{\rm O\ atom}(e^2/2mc^2)r^{-3}_{\rm Xe–O}, \quad (11)$$

where $(\frac{1}{3})\langle\rho^2\rangle_{\rm O\ atom}$ is proportional to the average diamagnetic susceptibility of the atom. Incidentally, they also provided the perpendicular diamagnetic shielding term,

$$\sigma_{\perp}^{\rm diam}(\mathrm{Xe–O})\approx\sigma_{\perp}^{\rm diam}(\text{free Xe atom}) + (e^2/2mc^2)Z_{\rm O}r^{-1}_{\rm Xe–O} - (\tfrac{1}{3})\langle\rho^2\rangle_{\rm O\ atom}(e^2/2mc^2)r^{-3}_{\rm Xe–O}, \quad (12)$$

where $Z_{\rm O}$ is the number of electrons of the O atom. Therefore, if we use the Flygare–Goodisman approximation for the diamagnetic shielding tensor components, we find

$$[\sigma_{\parallel}(\mathrm{Xe–O})-\sigma(\text{free Xe atom})] \approx +(\tfrac{2}{3})\langle\rho^2\rangle_{\rm O\ atom}(e^2/2mc^2)r^{-3}_{\rm Xe–O} \approx +28.180\ \text{ppm Å}^3 r^{-3}_{\rm Xe–O}, \quad (13)$$

$$[\sigma_{\perp}(\mathrm{Xe–O})-\sigma(\text{free Xe atom})] \approx +(\tfrac{3}{2})\sigma_{\rm iso}(\mathrm{Xe–O})-(\tfrac{1}{3})\langle\rho^2\rangle_{\rm O\ atom}(e^2/2mc^2)r^{-3}_{\rm Xe–O} \approx (\tfrac{3}{2})\sigma_{\rm iso}(\mathrm{Xe–O})-14.090\ \text{ppm Å}^3 r^{-3}_{\rm Xe–O}, \quad (14)$$

where $(\frac{1}{3})\langle\rho^2\rangle_{\rm O\ atom}$ is given by 1.0 Å^2 in their tables; the fundamental constants $(e^2/2mc^2)=14.090$ ppm Å. We can check the Flygare–Goodisman approximation against the *ab initio* calculations for Xe–Ne and Xe–Ar, for example, and we find that it is reasonably good. Here then, in Eqs. (13)–(14), is a possible recipe for obtaining the Xe shielding tensor from an empirical $\sigma_{\rm iso}(\mathrm{Xe–O_{zeol}})$ function of distance $r_{\rm Xe–O}$ in a zeolite. We do have a $\sigma_{\rm iso}(\mathrm{Xe–O_{zeol}})$ function for Xe in an alpha cage of zeolite Na*A*, which is an average over all the O atom types, derived from an *ab initio* calculation of the intermolecular shielding of a rare gas atom with fragments of the alpha cage.[56] This corresponds to a 1:1 Si/Al aluminosilicate crystal that has a rather different electronic structure of the O atoms than in an aluminum phosphate crystal, thus provides a different Xe shielding response. We can use this isotropic Xe shielding to make the dimer tensor functions as described in Eqs. (13) and (14), using the Flygare–Goodisman approximation. This model Xe–O dimer tensor provides another example that can be compared to the other model channels. In Fig. 6 and Fig. 7, we compare the Xe–channel intermolecular shielding tensors obtained by using this Xe–O dimer shielding tensor model with the others already discussed, to see the differences that arise from using various Xe–O dimer shielding tensor models. We have used a couple of V(Xe–O) potential functions: (a) the same potential as the V(Xe–Ar) scaled to $r_0=3.4$ Å [these results are shown in Figs. 6(b) and 7(b)], and (b) the same

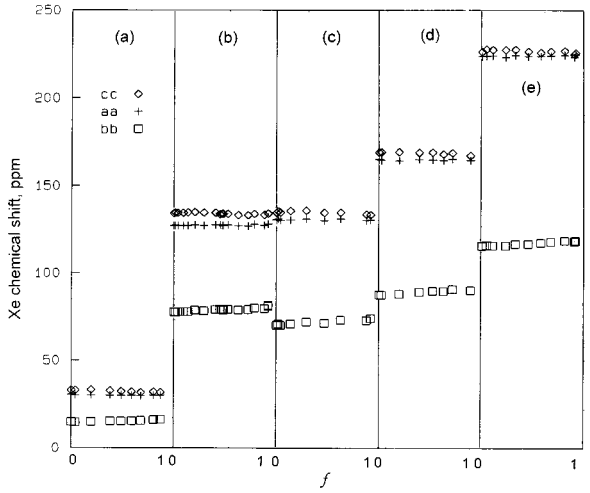

FIG. 7. The contribution of Xe–channel intermolecular interactions to the Xe chemical shift tensor, as a function of the Xe occupancy number in model channels of the ALPO-11 structure (a) consisting of Ne atoms, (b) consisting of O atoms characteristic of aluminosilicates with a 1:1 Si/Al ratio, (c) consisting of Ar-like atoms scaled down to $r_0=3.4$ Å, (d) scaled down to $r_0=3.5$ Å, and (e) consisting of Ar atoms.

Lennard–Jones potential that had been used for Xe in 1:1 aluminosilicates.[44] Using a specific σ(Xe–O) function, we find that in the limit of zero occupancy, a shorter $r_{\rm min}$ and a deeper potential well lead to Xe tensor components that are more deshielded relative to the free Xe atom. Both factors lead to Xe–O pair distribution functions that favor the highly deshielded values at short distances of the dimer tensor components perpendicular to the line of centers.

Figure 7 shows that the Xe–channel intermolecular shielding tensor remains largely unchanged as the Xe occupancy number in the channel is changed from nearly zero to maximum occupancy. The line shapes in Fig. 6 correspond to the first point (near $f=0$) in each case in Fig. 7. An examination of the numbers reveal that there are small but systematic trends that may be significant: Uniformly (in all cases from the Ne to the Ar channel and other models in between), chemical shift tensor components δ_{cc} and δ_{aa} slightly decrease, whereas component δ_{bb} slightly increases with increasing Xe occupancy. These small systematic changes with increasing occupancy can be attributed to small systematic changes in the Xe–O pair distribution functions with increasing occupancy. Nevertheless, these changes are small and for practical purposes it makes sense to think of the Xe–channel intermolecular shielding as largely invariant to the Xe occupancy number. This finding is in agreement with the original assumption made by Fraissard that the Xe isotropic chemical shift in a zeolite has an invariant surface contribution $\delta_{\rm surf}$ unaffected by the occupancy number.[57] This was found not to be the case for Xe trapped inside the cages of zeolite Na*A*.[44]

We examined the Xe–Xe part of the intermolecular shielding tensor that results from using various V(Xe–O) potential functions. We find that (a) the order of the components is invariant to the choice of the V(Xe–O) function used, and (b) the choice of r_0 has a significant effect on two components of the tensor, those two components perpendicu-

lar to the channel axis. To obtain the Xe–Xe contribution to the tensor, the *ab initio* Xe–Xe dimer shielding tensor as a function of the Xe–Xe distance is averaged over the configurations of Xe atoms in the channel. A large r_0 for V(Xe–O) effectively reduces the available volume for the Xe atoms, leading to a higher occurrence of the shorter Xe–Xe distances that correspond to steeply deshielded values of σ(Xe–Xe). Therefore, for a given channel structure such as ALPO-11, the proper choice of r_0(Xe–O) can be estimated from the change in anisotropy of the Xe–Xe part of the tensor with Xe occupancy. Given that we found that the Xe–channel part of the tensor is largely independent of occupancy in an ALPO-11 structure [for any reasonable choice of V(Xe–O) and σ(Xe–O), ranging from Xe–Ne to Xe–Ar], it is actually possible to deduce the Xe–Xe part of the tensor from the experimental spectra and compare these with the results of the GCMC simulations obtained in the model Ne or Ar channels shown in Fig. 4. A value in the vicinity of 3.4 Å is quite appropriate r_0 for Xe–O when the well depth is taken to be about the value appropriate for Xe–Ar. In all the GCMO simulations for this paper, the V(Xe–Xe) is fixed at the Maitland–Smith function fitted to the best empirical Xe–Xe potential function from Aziz and Slaman,[58] the same one that we have used in all our previous work on Xe in zeolites,[17,39,44,47,49,53,59–62] and the σ(Xe–Xe) is the function obtained from our *ab initio* calculations, multiplied by a factor 1.16 to agree with the density coefficients measured as a function of temperature in pure Xe gas.[16]

Using the various Xe–O models leads to the same qualitative behavior for the total tensor as a function of occupancy, clearly a signature of the ALPO-11 architecture. Differences from model to model are easily understood from the Xe–channel contributions and the Xe–Xe contributions separately, both changing in predictable systematic ways according to the Xe–O model used. The tensor appears pseudoaxially symmetric at two occupancies. When thermally polarized Xe is used, unless experiments are conducted over a range of occupancy numbers in a nanochannel, a false conclusion about the symmetry of the channel may result.

V. APPLICATION TO Xe IN ALPO-11

The nanochannels running parallel to the *c* axis of the ALPO-11 crystal provide a regular well-defined structure in which the Xe atoms can be found. The x-ray diffraction data provide the positions of Al, P, and O atoms in the crystal, and there are no ambiguities about partial occupations of atomic sites.[63] The cross-sectional area of the channels are such that, within a nanochannel, no more than one Xe atom may be found at any plane perpendicular to the *c* axis of the crystal. Assigning a typical van der Waals diameter (2.6 Å) to the oxygen atoms making up the channel walls leaves a cross section available to the Xe atom that is effectively 6.7 $\times$4.4 Å. This system provides an excellent case study since the pore space is effectively a one-dimensional elliptical cylinder, thus explicitly requires that the average Xe shielding tensor be nonaxial. There is only one type of oxygen atom since all the linkages are Al–O–P. These are the reasons we have used the ALPO-11 architecture for our Ne and Ar channels. At this point, we are in a position to consider the Xe NMR line shapes in the channels of the actual ALPO-11 crystal itself.

In a series of very careful experiments, Ripmeester and Ratcliffe have systematically studied the Xe NMR line shapes in ALPO-11 for the entire range of possible Xe occupancies, under carefully controlled conditions of temperature and other variables.[35] From these line shapes they extracted the set of average Xe shielding tensor components at ten different Xe occupancies ranging from 9.6% to 100% of the maximum occupancy of 16.40×10^{-4} moles Xe/g of dry ALPO-11. The latter corresponds to four Xe atoms per unit cell. The experiments did not provide the assignment of the tensor components to the axis system of the channel, but the systematic studies did provide the correlation of tensor components from one occupancy to another. Thus, Ripmeester and Ratcliffe found that one component of the average chemical shift tensor of Xe did not change with occupancy (within experimental error), whereas each of the other two components increased systematically with occupancy, albeit with different slopes. At the half-full occupancy (two Xe per unit cell), the experimental average chemical shift tensor appears axially symmetric.

Using the model Xe–O_{zeol} dimer shielding tensor functions, we have carried out the GCMC simulations of Xe in ALPO-11. The results are shown in Fig. 8. By modifying the potential functions V(Xe–O) and modifying the dimer shielding function σ(Xe–O), we could conceivably arrive at a better match with experiment. We do not attempt a fit to experiment here. Instead, we used one [that one used for Figs. 6(b) and 7(b)] of several reasonable choices of V(Xe–O) and we used the dimer shielding tensor function derived from the (Na,K,Ca)A zeolite fragments using Eqs. (13)–(14). Other choices of V(Xe–O) and σ(Xe–O) [using the Lennard–Jones potential parameters used in Xe/NaA,[44] for example, and those simulations that appear in Fig. 7(c)] lead to semiquantitatively the same series of spectra as shown in Fig. 8. We can compare these simulated spectra with the experimental results of Ripmeester and Ratcliffe that are reproduced in Fig. 9. We find the agreement satisfactory. The variation of the tensor components with occupancy is given in Fig. 10(c) for a comparison with the experimental data of Ripmeester and Ratcliffe in Fig. 10(b). We also show in Fig. 10(a) the GCMC results using shielding and potential functions for Ar-like channel atoms scaled to $r_0=3.4$ Å [these functions were used in the GCMC results shown in Figs. 6(c) and 7(c)]. Figure 10 shows that both sets of shielding functions give a reasonably good agreement with experiment. Having separated the Xe–channel and the Xe–Xe parts of the average shielding tensor, it is straightforward to understand the systematic changes in the experimental Xe line shapes in ALPO-11 as Xe occupancy increases from near zero to full occupancy. While their experiments did not permit the assignments of the tensor components to the crystal axes, our simulations with model systems of Ne and Ar atoms do permit such unequivocal assignments that do not depend on the model function used for the σ (Xe–O_{zeol}) tensor. The labels that we have attached to the

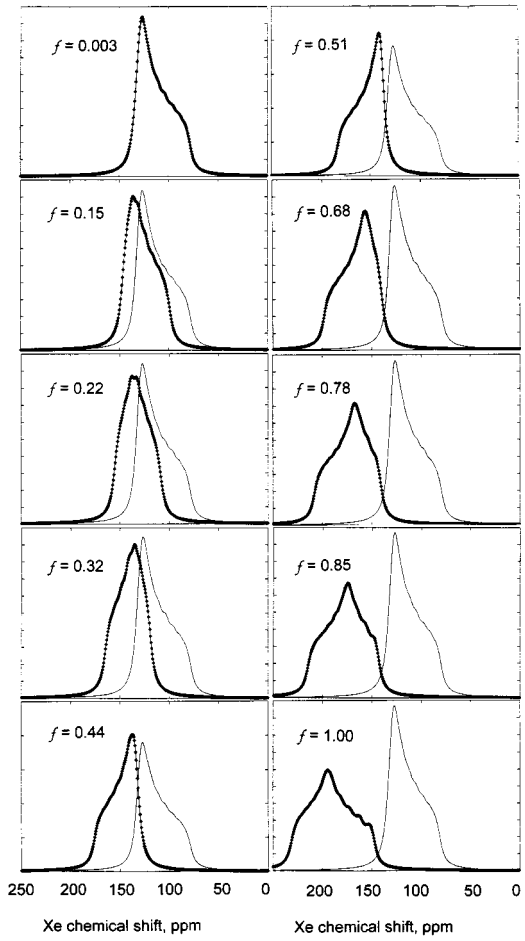

FIG. 8. Xe NMR line shapes from GCMC simulations as a function of occupancy of Xe in ALPO-11. The Xe–channel contribution (shown without points) is displayed together with the total spectrum (shown with points). Occupancies are shown as fractions of maximum occupancy (four Xe atoms per unit cell).

components in Figs. 10(a) and 10(c), and all other labels *aa,bb,cc* used in this paper for the principal axes of the shielding tensor do correspond to the crystalline axis labels for ALPO-11. Experiments could not provide the unequivocal assignment of the average tensor components to the axis system, but Ripmeester and Ratcliffe correctly assigned the nearly constant component of the average tensor to the *cc* component.[35]

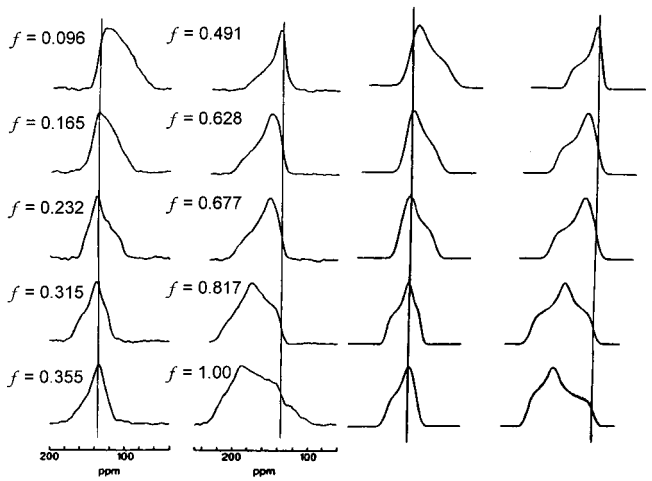

FIG. 9. Experimental Xe NMR line shapes in ALPO-11 from Ripmeester and Ratcliffe (Ref. 35). Their fit to the experimental spectra are shown on the right.

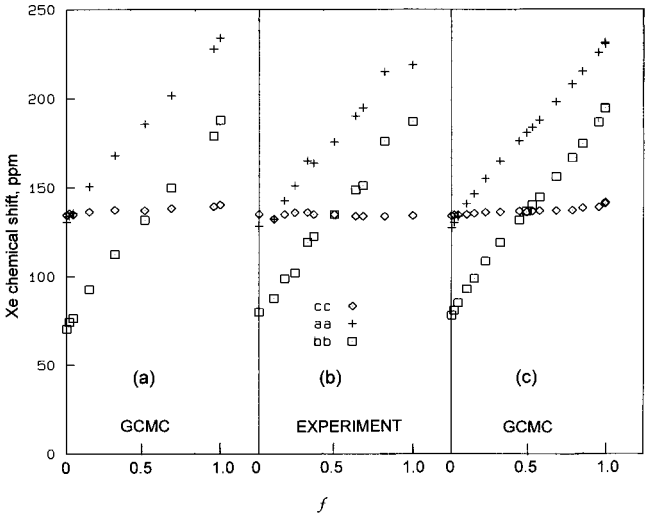

FIG. 10. Average chemical shift tensor components for the Xe atom from GCMC simulations in an ALPO-11 structure are shown in (a) and (c), compared with (b) from experiments on Xe in ALPO-11 by Ripmeester and Ratcliffe (Ref. 35). The model channel in (a) consists of Ar-like atoms scaled down to $r_0 = 3.4$ Å, in (c) consists of atoms characteristic of aluminosilicates with a 1:1 Si/Al ratio. The same potential function is used in the GCMC simulations for both (a) and (c), only the Xe–O shielding function is different.

Ripmeester and Ratcliffe[35] were the first to consider the observed shielding tensor as a property of the distribution of sorbate atoms in a channel. In the analysis of their experimental lineshapes, Ripmeester and Ratcliffe used a simple model of Xe atoms distributed among the four adsorption sites per unit cell. They assumed a binomial distribution of M atoms into K sites. In the limit $K \to \infty$ at an average Xe occupancy of $f = M/K$, the fraction of sites that are occupied, with both neighbors unoccupied is $(1-f)^2$; the fraction of sites that are occupied with one neighboring site likewise occupied is $2f(1-f)$ and the fraction of sites that are occupied with both neighbors occupied is f^2. A rapid exchange of the Xe atoms among the adsorption sites then brings about dynamic averaging of the components of the three chemical shift tensors, weighted by, respectively, $(1-f)^2$, $2f(1-f)$, and f^2:

$$\langle \delta_{\alpha\alpha} \rangle = (1-f)^2 \delta_{\alpha\alpha}(\mathrm{I}) + 2f(1-f)\delta_{\alpha\alpha}(\mathrm{II}) + f^2 \delta_{\alpha\alpha}(\mathrm{III}), \tag{15}$$

where $\delta_{\alpha\alpha}$ (I, II, and III) are constants deduced from experiment. Their simple model works well enough to account for the approximately linear dependence on f of each of the tensor components that could be obtained from the line shape fitting of each spectrum. Our GCMC simulations do produce the three nearly straight lines similar to their experimental results. However, the physical picture associated with their model and our GCMC simulations are rather different. In our work the distribution of Xe atoms inside the channel are not assumed. Rather, the Xe distributions are a direct consequence of the GCMC simulations. The Xe positions can be

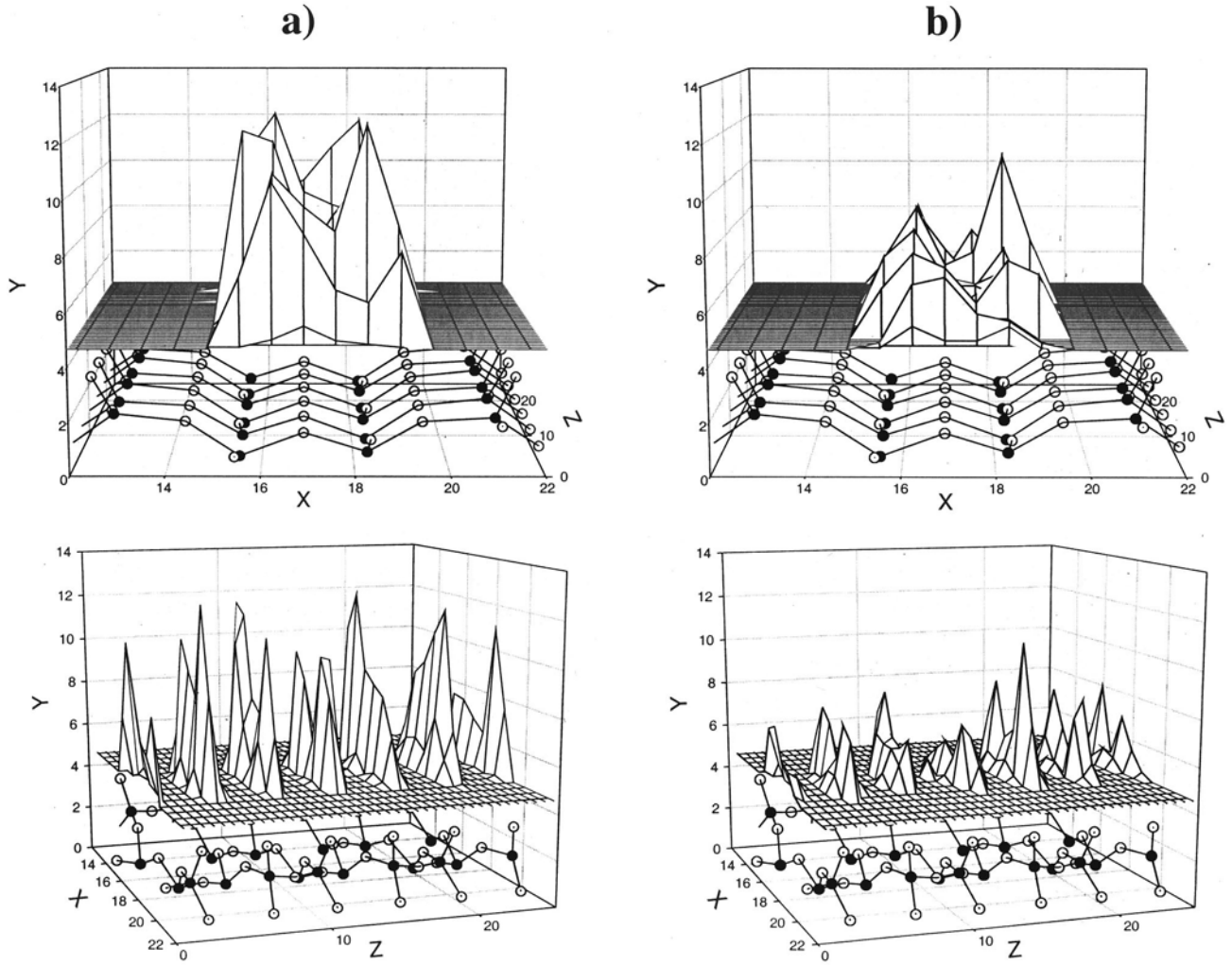

FIG. 11. Two views of the one-body distribution functions for Xe in ALPO-11 at $y=4.62$ Å for (a) nearly full occupancy, and for (b) 0.26% occupancy, are shown for one of the channels in three unit cells stacked along the z axis. The x, y, and z axes of our simulation box are along the a, b, c axes of the crystal. For clarity, only a portion of the channel structure is shown. The dark atoms are Al or P atoms, while the open circles are O atoms.

anywhere within the channel; they are not limited to the adsorption sites; the only constraint on the number of Xe atoms within the channel and their configurations is the requirement that the Xe chemical potential in the channel be the same as the bulk Xe with which the ALPO-11 sample is at equilibrium, at the same temperature, at a constant volume.

The GCMC simulations provide a one-body Xe distribution function. We illustrate this distribution function in the plane containing the lowest-energy sites for Xe in ALPO-11. In each of two channels in a unit cell there are two sets of two adsorption sites into which at most two Xe atoms are distributed at full occupancy. These four sites were found at $y=4.62$ Å (x,y, and z axes are along the a,b,c crystalline axes, respectively). Thus, in Fig. 11 we show, in the plane $y=4.62$ Å within a channel in three unit cells stacked along the z axis, a typical distribution function obtained for nearly full occupancy ($f\approx 1$) and at 0.26% occupancy ($f=0.0026$) at 300 K. We note that these are not delta function distributions; the Xe atoms are significantly localized but there is also a fair amount of delocalization. We can see positions of high probability of finding a Xe atom, but the one-body distribution function does not correspond to individual sharp peaks located only at the 12 adsorption sites. We see that for both the nearly empty and the fully occupied channel at 300 K, although the distribution is fairly narrow in the plane $y=4.62$ Å, there is considerable sloshing around along the x direction.

It would be interesting to find the static shielding tensors associated with each of the site types suggested by Ripmeester and Ratcliffe.[35] We note here that Ripmeester and Ratcliffe did not assume Xe atoms were static at adsorption sites; rather they envisioned the tensors that they assigned to three site types as already average values within cells or the immediate vicinity of the adsorption sites. Our purpose in comparing static to fully averaged tensors is to discover the extent to which the static tensor components are modified by the excursions of the Xe atoms away from the lowest-energy sites at room temperature. We found two inequivalent adsorption sites for a single Xe in ALPO-11, which we labeled A and B, in increasing order of energy. There are two sets of these in each channel of the unit cell. Adjacent A and B sites are side by side at the same z (along c), separated by only 2.58 Å along the x (a) direction. The next set of sites are B

TABLE II. Static Xe chemical shift tensors calculated for the three site types proposed by Ripmeester and Ratcliffe (Ref. 35): Xe at a minimum energy adsorption site and ○ corresponds to no Xe atoms at neighbor sites. The Xe chemical shift tensors, $\delta_{\alpha\alpha}=[\sigma(\text{free Xe atom})-\langle\sigma_{\alpha\alpha}\rangle]$, for the static configuration of site types are compared with the GCMC averages for corresponding occupancies; all are calculated in this work, using the same potential and shielding functions for static and averaged values.

Adsorption site	Static Static site types	Chemical shift tensors, ppm δ_{cc}	δ_{aa}	δ_{bb}
A	I ○Xe○	145.2	138.7	93.6
	II ○XeXe	144.6	147.5	106.4
	III XeXeXe	142.3	155.7	117.9
B	I ○Xe○	134.8	124.5	90.9
	II ○XeXe	134.8	139.2	112.0
	III XeXeXe	132.9	152.8	130.6
Average of static values				
	I ○Xe○	140.0	131.6	92.2
	II ○XeXe	139.7	143.4	109.2
	III XeXeXe	137.6	154.2	124.3
	$\frac{1}{4}$I+$\frac{1}{2}$II+$\frac{1}{4}$III	139.2	143.1	108.7
GCMC average	Fractional occupancy	δ_{cc}	δ_{aa}	δ_{bb}
	$f=0.0$	134.2	127.1	77.6
	$f=0.500$	136.4	181.8	138.0
	$f=1.000$	141.2	231.2	194.6

and A sites, midway (4.186 Å) along the channel axis. We placed a single Xe at one of the lowest-energy positions for Xe in ALPO-11, with no Xe neighbors (the Ripmeester and Ratcliffe site type I or ○Xe○) and calculated the static shielding tensors in this configuration. We also placed two Xe atoms initially at adjacent lowest-energy positions for a single atom with no other neighbors (their site type II or ○XeXe), minimized the total energy, and calculated the static shielding tensor. Finally, we placed three Xe atoms initially at adjacent lowest-energy positions for single atoms, minimized the total energy and calculated the static shielding tensors at the energy-optimized Xe positions. The results are shown in Table II for Xe in the adsorption sites. We compare the static values for the single Xe atom at an adsorption site with the average shielding tensor obtained from GCMC simulations (which are averages over a large number of appropriately weighted configurations, the most energetically favorable ones being the static ones). The same V(Xe–O) and σ(Xe–O) functions have been used for the static and GCMC averaged calculations in Table II. For nearly zero occupancy, that is, no more than one Xe atom per channel, the static type I shielding tensor for adsorption site A is the one that would be observed at extremely low temperatures. On the other hand, the average shielding tensor at room temperature would include configurations other than the most energetically favorable one, and it is the former rather than the latter that Ripmeester and Ratcliffe identify with their site I tensor in their Table 2.[35]

We see in Table II that the Xe chemical shift tensor for the Xe in isolated singles (○Xe○) has an average that is different from the GCMC-averaged shift tensor at nearly zero occupancy, but the differences are small for all but the δ_{bb} (which corresponds to the principal component in the cross-sectional plane and along the short axis of the ellipse). The static value (92.2 ppm) is larger than the GCMC average δ_{bb} value (77.6 ppm). This is easily understood when we note that there is considerable latitude in the positions the Xe may take in the plane perpendicular to the *b* axis, as seen very clearly in the one-body distribution function shown in Fig. 11, due to the elongated cross section. Thus, the Xe may explore positions farther away from the lowest-energy sites at the walls of the channel, and those locations correspond to less deshielding or lower chemical shifts. On the other hand, there is very little room for exploration along the other direction in the cross-sectional plane, since the ''free'' diameter of the channel along that direction is only 4.4 Å, thus the static value for δ_{aa} (131.6 ppm) is close to the GCMC-averaged value (127.1 ppm) in the limit of $f=0$. Comparing the chemical shift tensor of the middle Xe in static triples (XeXeXe), that are in adjacent adsorption sites, with the GCMC-average chemical shift tensors in the limit of maximum occupancy, $f=1.0$, we find that the static values are considerably smaller for both δ_{aa} and δ_{bb} (154.2 and 124.3 ppm, respectively), compared to the GCMC average values (231.2 and 194.6 ppm). In fact, none of the static tensors at adsorption sites have δ_{aa} and δ_{bb} as large as 231.2 and 194.6 ppm, respectively, the largest static values being 155.7 and 130.6 ppm. The physical basis for the difference between the GCMC averages and the average over static adsorption sites is the following: There is no arithmetic-or energy-weighted average over only the adsorption sites that can give rise to the correct Xe–Xe interactions because the lowest-energy arrangement places the Xe atoms into sites that are in fixed distances from each other in a fully occupied channel. At these distances, the static values calculated are too small because the Xe–Xe contributions are smaller than they would be at room temperature, at which the less favorable configurations having shorter Xe–Xe distances, that have correspondingly highly deshielded values, are sampled by the system. This is observed in the Xe–Xe pair distribution function from the GCMC simulations that are not shown here. Since Xe–Xe contributions to δ_{cc} are very small compared to the δ_{aa} and δ_{bb} components (as seen in Fig. 4), the static value for δ_{cc} (137.6 ppm) is reasonably close to the GCMC average value, even at $f=1.00$ (141.2 ppm). The differences found here between the static and GCMC-averaged chemical shifts are not as large as those found in the case of Xe atoms at high occupancy in alpha cages of Na*A* zeolite.[53]

The sum of static tensors $\frac{1}{4}$ type I+$\frac{1}{4}$ type III+$\frac{1}{2}$ type II is compared with the GCMC-average shielding tensor at 300 K at half-occupancy in Table II. The arithmetic average over the static singles, doubles, and triples is different from the GCMC average shift tensor at very close to half the maximum occupancy ($f=0.500$). The average of two out of three static tensor components at half-occupancy is significantly different from the GCMC average: 143.1 ppm instead of 181.8 ppm for δ_{aa}, 108.7 ppm instead of 138.0 ppm for δ_{bb}. In the half-occupied channel, just as in the fully occupied channel, the static components are less deshielded (smaller chemical shifts) since the GCMC average includes energetically less favorable configurations of shorter Xe–Xe distances that correspond to greater deshielding contributions. Because of this, the Xe tensors for the isolated Xe singles, doubles, and triples that are static in the adsorption sites

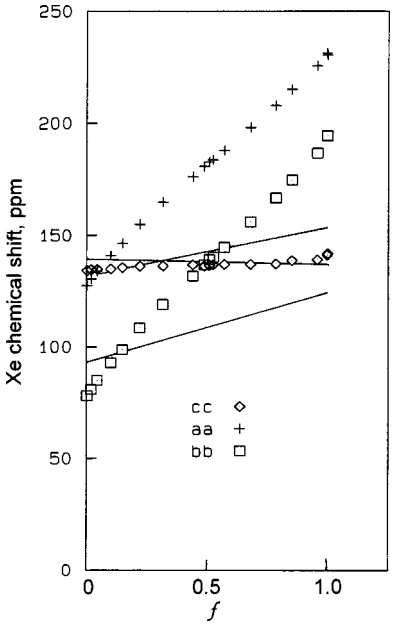

FIG. 12. The lines correspond to the average shielding tensor components that would be obtained using Eq. (15) based on a binomial distribution of Xe among adsorption sites, where the $\delta_{\alpha\alpha}$ (I), $\delta_{\alpha\alpha}$ (II), and $\delta_{\alpha\alpha}$ (III) are identified with the static values at those sites (given in Table II), whereas the points correspond to the GCMC averages [the same as in Fig. 10(c)], using the same potential functions and shielding tensor functions for both static and GCMC averages.

should be quite different from the average chemical shift tensors extracted from the experimental spectra at empty, half-full, and full occupancy. In Fig. 12 we plot the average chemical shift tensor components that would be obtained from Eq. (15) if the $\delta_{\alpha\alpha}$ (I), $\delta_{\alpha\alpha}$ (II), and $\delta_{\alpha\alpha}$ (III) are identified with the static values given in Table II. There is a difference between (1) the GCMC-average tensors (shown as points) obtained from simulations having Xe distributions in the channel such as those shown in Fig. 11, and (2) the average tensors (shown as lines) that would have been obtained from Eq. (15) by replacing Fig. 11 with a binomial distribution of Xe atoms into adsorption sites.

In the Ripmeester and Ratcliffe model for Xe in ALPO-11, the dynamic averaging of the Xe chemical shift tensor was taken into account by taking the sum over only three site types, as in Eq. (15). On the other hand, the GCMC simulation sums over a very large number of configurations in which the individual Xe atoms are permitted to take positions *other than the minimum energy sites*, constrained only by the condition that the chemical potential of Xe in the channel be equal to that in the bulk gas, and the shielding tensor for each Xe is calculated for each configuration. The one-body distribution functions for Xe in the ALPO-11 structure in Fig. 11 show that the Xe atoms are not very localized. At room temperature, the Xe has a distribution function that is fairly smeared out, not at all like delta functions at the adsorption sites. Thus, we find that although the Ripmeester and Ratcliffe main idea that the observed line shape is a function of the distribution of Xe atoms in the channel is correct and was an important step toward the physical interpretation of the observed Xe line shapes in nanochannels, in general, the model of binomial distributions of Xe atoms into distinct adsorption sites is oversimplified.

VI. CONCLUSIONS

We have demonstrated that the new approach that we call the *additive dimer tensor model* can successfully be used to generate the shielding tensor component along an arbitrary direction in the laboratory-fixed (simulation box-fixed) axes, as a function of configuration for a Xe atom among other Xe atoms in a nanochannel of atoms fixed at crystallographic locations. We demonstrated the use of this model by creating nanochannels with the architecture of ALPO-11, constituted by Ne atoms or Ar atoms. With these model channels, we systematically explored a variety of questions and obtained answers that provide general insight into what exactly does the Xe anisotropic line shapes reveal about the nanochannel, what types of line shape changes may be expected as the Xe occupancy is increased from zero to full occupancy, and what types of line shape changes may be expected as the constituent atoms of the channel are changed. By using model Ne and Ar channels, and separately investigating at the Xe–channel and Xe–Xe contributions to the NMR spectrum, the various factors that influence the Xe chemical shift tensor are individually explored. Experimental spectra include all the contributions together and is made more easily analyzable in terms of these model calculations. The tuning of the Xe–O shielding tensor function within the range Ne channel to Ar channel provides insight into the magnitudes of differences that may be expected in the Xe NMR spectrum when the electronic structure of the channel changes, while the architecture remains the same.

Finally, an actual experimental system is considered and the spectral simulation method developed here is applied to the Xe NMR lineshapes of Xe in ALPO-11 crystallites under a systematic variation in Xe occupancy from nearly zero occupancy to full occupancy. The understanding had already been provided by the model channels. What finally is achieved here is in excellent comparison with the experimental spectra. However, the more important conclusions arise from the model channel studies: the variations in line shape are all well understood in terms of the Xe–channel contributions separately from the Xe–Xe contributions. In the final analysis, the potential function used to describe the interaction between Xe and the channel atoms is not particularly important. The qualitative systematic changes in these contributions provide the signature of a nanochannel with an elliptical cross section, and are independent of the atoms constituting the channel.

ACKNOWLEDGMENTS

This research was supported by National Science Foundation Grant No. CHE99-79259 for which the author is very grateful. This work has been inspired by the excellent Xe NMR line shape studies of J. A. Ripmeester, C. I. Ratcliffe, and co-workers from 1981 to the present. The author is grateful to Devin Sears and Vivek Shah for preparing Fig. 11 from the one-body distribution results.

[1] C. J. Jameson, Chem. Rev. **91**, 1375 (1991).
[2] A. C. de Dios and C. J. Jameson, in *Annual Reports on NMR Spectroscopy*, edited by G. A. Webb (Academic, London, 1994), Vol. 29, pp. 1–69.
[3] C. J. Jameson and H. J. Osten, in Ref. 2, Vol. 17, pp. 1–78.
[4] C. J. Jameson, in *Isotopes in the Physical and Biomedical Sciences*, Vol. 2, Isotopic Applications in NMR Studies, edited by E. Buncel and J. R. Jones (Elsevier, Amsterdam, 1991), Chap. 1, pp. 1–54.
[5] C. J. Jameson, in *Theoretical Models of Chemical Bonding, Molecular Spectroscopy, Electronic Structure, and Intramolecular Interactions*, edited by Z. B. Maksic (Springer-Verlag, Berlin, 1991), Part 3, pp. 457–519.
[6] A. K. Jameson, C. J. Jameson, and H. S. Gutowsky, J. Chem. Phys. **53**, 2310 (1970).
[7] C. J. Jameson, A. K. Jameson, and S. M. Cohen, J. Chem. Phys. **62**, 4224 (1975).
[8] C. J. Jameson, A. K. Jameson, and S. M. Cohen, J. Chem. Phys. **65**, 3401 (1976).
[9] C. J. Jameson, A. K. Jameson, and S. M. Cohen, J. Chem. Phys. **66**, 5226 (1977).
[10] T. R. Stengle, N. V. Reo, and K. L. Williamson, J. Phys. Chem. **85**, 3772 (1981).
[11] T. R. Stengle, S. M. Hosseini, and K. L. Williamson, J. Solution Chem. **15**, 777 (1986).
[12] J. B. Miller, J. H. Walton, and C. M. Roland, Macromolecules **26**, 5602 (1993).
[13] T. R. Stengle and K. L. Williamson, Macromolecules **20**, 1428 (1987).
[14] D. Raftery, L. Reven, H. Long, A. Pines, P. Tang, and J. A. Reimer, J. Phys. Chem. **97**, 1649 (1993).
[15] J. H. Kantola, J. Vaara, T. T. Rantala, and J. Jokisaari, J. Chem. Phys. **107**, 6470 (1997).
[16] A. C. de Dios, D. Sears, and C. J. Jameson (unpublished).
[17] C. J. Jameson, A. K. Jameson, P. Kostikin, and B. I. Baello, J. Chem. Phys. **112**, 323 (2000).
[18] A. C. de Dios and C. J. Jameson, J. Chem. Phys. **107**, 4253 (1997).
[19] J. L. Bonardet, J. Fraissard, A. Gedeon, and M. A. Springuel-Huet, Catal. Rev. Sci. Eng. **41**, 115 (1999).
[20] C. I. Ratcliffe, *Annual Reports on NMR Spectroscopy*, edited by G. A. Webb (Academic, London, 1998), Vol. 36, pp. 123–221.
[21] T. Pietrass, Magn. Reson. Rev. **17**, 263 (2000).
[22] C. Dybowski, N. Bansal, and T. M. Duncan, Annu. Rev. Phys. Chem. **42**, 433 (1991).
[23] D. Raftery and B. F. Chmelka, *NMR Basic Principles and Progress*, edited by P. Diehl, E. Fluck, H. Guenther, R. Kosfeld, and J. Seelig (Springer-Verlag, Berlin, 1994), Vol. 30, pp. 111–158.
[24] J. M. Kneller, R. J. Soto, S. E. Surber, J. F. Colomer, A. Fonseca, J. B. Nagy, G. van Tendeloo, and T. Pietrass, J. Am. Chem. Soc. **122**, 10591 (2000).
[25] Y. Q. Song, B. M. Goodson, R. E. Taylor, D. D. Laws, G. Navon, and A. Pines, Angew. Chem. Int. Ed. Engl. **36**, 2368 (1998).
[26] M. Luhmer, B. M. Goodson, Y. Q. Song, D. D. Laws, L. Kaiser, M. C. Cyrier, and A. Pines, J. Am. Chem. Soc. **121**, 3502 (1999).
[27] H. Desvaux, T. Gautier, G. Le Goff, M. Petro, and P. Berthault, Eur. Phys. J. D **12**, 289 (2000).
[28] C. Landon, P. O. Berthault, F. Vovelle, and H. Desvaux, Protein Sci. **10**, 762 (2001).
[29] J. A. Ripmeester, J. Magn. Reson. **56**, 247 (1984).
[30] J. A. Ripmeester, J. Am. Chem. Soc. **104**, 289 (1982).
[31] D. W. Davidson, Y. P. Handa, and J. A. Ripmeester, J. Phys. Chem. **90**, 6549 (1986).
[32] C. J. Jameson and A. C. de Dios, J. Chem. Phys. **116**, 3805 (2002).
[33] J. A. Ripmeester, C. I. Ratcliffe, and J. S. Tse, J. Chem. Soc., Faraday Trans. 1 **1988**, 3731.
[34] J. A. Ripmeester and D. W. Davidson, J. Mol. Struct. **75**, 67 (1981).
[35] J. A. Ripmeester and C. I. Ratcliffe, J. Phys. Chem. **99**, 619 (1995).
[36] J. A. Ripmeester and C. I. Ratcliffe, Mater. Res. Soc. Symp. Proc. **233**, 281 (1991).
[37] M. A. Springuel-Huet and J. Fraissard, Chem. Phys. Lett. **154**, 299 (1989).
[38] P. Sozzani, A. Comotti, R. Simonutti, T. Meersmann, J. W. Logan, and A. Pines, Angew. Chem. Int. Ed. Engl. **39**, 2695 (2000).
[39] C. J. Jameson, A. K. Jameson, R. E. Gerald II, and H. M. Lim, J. Phys. Chem. B **101**, 8418 (1997).
[40] I. L. Moudrakovski, V. V. Terskikh, C. I. Ratcliffe, and J. A. Ripmeester, *42nd Experimental NMR Conference*, 11–16 March 2001, Orlando.
[41] I. L. Moudrakovski, C. I. Ratcliffe, and J. A. Ripmeester, Appl. Magn. Reson. **10**, 559 (1996).
[42] I. L. Moudrakovski, A. Nossov, S. Lang, S. R. Breeze, C. I. Ratcliffe, B. Simard, G. Santyr, and J. A. Ripmeester, Chem. Mater. **12**, 1181 (2000).
[43] I. L. Moudrakovski, A. Nosso, S. Lang, C. I. Ratcliffe, J. A. Ripmeester, *NMR Symposium*, 42nd Rocky Mountain Conference, Broomfield, CO, 30 July–3 August, 2000.
[44] C. J. Jameson, A. K. Jameson, B. I. Baello, and H. M. Lim, J. Chem. Phys. **100**, 5965 (1994).
[45] A. E. Hansen and T. D. Bouman, J. Chem. Phys. **91**, 3552 (1989).
[46] C. P. Slichter, *Principles of Magnetic Resonance*, 3rd ed. (Springer-Verlag, Berlin, 1989), p. 606.
[47] C. J. Jameson, A. K. Jameson, A. C. de Dios, R. E. Gerald II, H. M. Lim, and P. Kostikin, in *Modeling NMR Chemical Shifts: Gaining Insights into Structure and Environment*, ACS Symposium Series 732, edited by J. C. Facelli and A. C. de Dios (Oxford University Press, Oxford, 1999), pp. 335–348.
[48] M. Mezei, Mol. Phys. **40**, 901 (1980).
[49] C. J. Jameson, A. K. Jameson, and H. M. Lim, J. Chem. Phys. **104**, 1709 (1996).
[50] M. P. Allen and D. J. Tildesley, *Computer Simulation of Liquids* (Clarendon, Oxford, 1987).
[51] D. A. Barrow, M. J. Slaman, and R. A. Aziz, J. Chem. Phys. **91**, 6348 (1989).
[52] R. A. Aziz and A. van Dalen, J. Chem. Phys. **78**, 2402 (1983).
[53] C. J. Jameson, A. K. Jameson, H. M. Lim, and B. I. Baello, J. Chem. Phys. **100**, 5977 (1994).
[54] N. F. Ramsey, Phys. Rev. **78**, 699 (1950).
[55] W. H. Flygare and J. Goodisman, J. Chem. Phys. **49**, 3122 (1968).
[56] C. J. Jameson and H.-M. Lim, J. Chem. Phys. **103**, 3885 (1995).
[57] J. Fraissard and T. Ito, Zeolites **8**, 350 (1988).
[58] R. A. Aziz and M. J. Slaman, Mol. Phys. **57**, 825 (1986).
[59] C. J. Jameson, A. K. Jameson, R. E. Gerald II, and H.-M. Lim, J. Chem. Phys. **103**, 8811 (1995).
[60] C. J. Jameson and H. M. Lim, J. Chem. Phys. **107**, 4373 (1997).
[61] C. J. Jameson, A. K. Jameson, and H. M. Lim, J. Chem. Phys. **107**, 4364 (1997).
[62] C. J. Jameson, H. M. Lim, and A. K. Jameson, Solid State Nucl. Magn. Reson. **9**, 277 (1997).
[63] J. M. Bennett, J. W. Richardson, Jr., J. J. Pluth, and J. V. Smith, Zeolites **7**, 160 (1987).